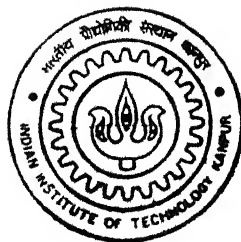


Development of Nickel and Nickel-Titanium substituted Barium Hexaferrites for Information Storage

By
MINI GROVER

TH
MS/2000/M
G1919 d



**MATERIALS SCIENCE PROGRAMME
INDIAN INSTITUTE OF TECHNOLOGY KANPUR
July, 2000**

Development of Nickel and Nickel-Titanium substituted Barium Hexaferrites for Information Storage

2000

A Thesis submitted
in partial fulfillment of the requirement
for the Degree of

Master of Technology

by

Mini Grover



Materials Science Programme

INDIAN INSTITUTE OF TECHNOLOGY, KANPUR

JULY, 2000

6 OCT 2000 / 1999

CENTRAL LIBRARY
A.T.T. KAMPUR

A132015

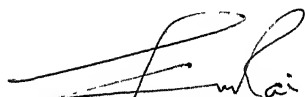


A132015

Submitted on 19.7.2000
R.

CERTIFICATE

It is certified that the work contained in this thesis entitled
“Development of Nickel and Nickel-Titanium substituted Barium Hexaferrites for Information Storage”, by **Mini Grover** has been carried out under my supervision and this work has not been submitted elsewhere for a degree.



(K.N. Rai)

Professor

Materials Science Programme
and Department of Material and
Metallurgical Eng.
Indian Institute of Technology
Kanpur (UP)-208016

Jitendra Kumar

(Jitendra Kumar)

Professor

Materials Science Programme
Indian Institute of Technology
Kanpur (UP)-208016

July, 2000

*DEDICATED TO,
My Parents
&
Rajeev, Lovely*

Acknowledgement

I expressed my sincere gratitude to my supervisors Prof. Jitendra kumar and Prof. K.N.Rai for their inspiring guidance during the course of thesis work. I am very fortunate that as I had been under their tutelage. Both constantly encouraged me and the freedom that I got was absolutely remarkable.

My sincere gratitude to Dr. H.C. Verma for his invaluable guidance and continuous encouragement during the course of investigation.

I am also thankful to Mr. D.K Rai and Mr. Chandan Upadhaya for introducing me in this very subject and help me out whenever required.

I am very grateful to Sanjeev, Shiv Govind bhaiya and Pankaj bhaiya, Nisha di, Latika, Sarika, Manisha, Parimal, Rajeev bhaiya and Arvind for their moral support and help towards the completion of this work.

I would like to give thanks my friends S.Srikanth, Amit Srivastava, Saibaba and Ramanujam maintaining the cordial and friendly environment throughout the course period and thereafter. I would like to extend my sincere thanks to Kalpna, Shikha, Savita, Deepa, Nidhi, Atul, Arun, Sharad, Pankaj and Manoj for their constant support and encouragement.

I appreciate Thapa ji and Abhishek kumar Srivastava for their timely help during my experiment work.

I am giving special thanks to Uma shankerji, Sharma ji and Agnihotriji for their constant help through out the experiments.

Thanks are due to my friends who gave a memorable and enjoyable company throughout my stay here.

The financial assistance provided by C.S.I.R is thankfully acknowledged.

Mini Grover

ABSTRACT

Nickel and nickel-titanium containing barium hexaferrite of composition $\text{BaFe}_{12-x}\text{Ni}_x\text{O}_{19-x/2}$ ($0 \leq x \leq 1.6$) and $\text{BaFe}_{12-2x}\text{Ni}_x\text{Ti}_x\text{O}_{19}$ ($0 \leq x \leq 1.0$) have been prepared by auto-ignition method and studied with regard to their phase(s), magnetic characteristics (specific magnetization, coercivity and Curie temperature) and Mossbauer spectra. It is shown that $\text{BaFe}_{12-x}\text{Ni}_x\text{O}_{19-x/2}$ maintains magnetoplumbite type hexagonal structure up to $x=0.6$, but, another phase of composition NiFe_2O_4 also emerges progressively in increasing amount for $x > 0.6$. Coercivity (H_c) and saturation magnetization (M_s) decrease with increase in nickel content (x) and their values correspond to 4300 and 1379 Oe, and 59.3 and 43.4 emu/g for $x=0$ and $x=1.6$, respectively. But the Curie temperature (T_c) increases and is found to be 458 °C and 474 °C for composition corresponding to $x=0$ and 1.4, respectively. Based on Mossbauer spectra, it is shown that nickel ions occupy 12k and 2b crystallographic sites preferentially and at $4f_{vi}$, $4f_{iv}$ and/or 2a sites randomly with rise in nickel content.

Nickel-titanium substituted barium hexaferrites of composition $\text{BaFe}_{12-2x}\text{Ni}_x\text{Ti}_x\text{O}_{19}$ with $0 \leq x \leq 1.0$ exhibit a single phase magnetoplumbite type hexagonal structure. Coercivity (H_c) is found to decrease steadily from 4300 to 1301 Oe, however, the saturation magnetization varies randomly but lie in the range 52-59.3 emu/g as Ni-Ti content (x) increases from 0 to 1.0. Curie temperature is shown to drop drastically and corresponds to 458 and 340° C for $x=0$ and 1.0 respectively. The

Mossbauer spectra indicate that Ni^{2+} and Ti^{4+} ions preferentially assume 12k, 2a and 2b crystallographic sites.

Finally it is pointed out that by adjusting Ni^{2+} and Ti^{4+} ions content (x), it is possible to obtain $\text{BaFe}_{12-2x}\text{Ni}_x\text{Ti}_x\text{O}_{19}$ compounds of suitable characteristics for information storage applications. e.g., products with $x=0.2-1.0$ exhibit coercivity and saturation magnetization in the range of 3000-1301 Oe and 52-58.4 emu/g.

CONTENTS

Certificate.....	ii
Acknowledgement.....	iii
Abstract	iv
Contents.....	vi
List of figures.....	ix
List of tables.....	xii
1. INTRODUCTION.....	1
1. Types of Recording.....	2
1.2 Requirements of recording medium.....	4
1.3 Materials for magnetic recording.....	7
1.4 Barium ferrite	10
1.5 Synthesis methods.....	15
1.6 Objective of present work.....	16
2. EXPERIMENTAL DETAILS.....	18
2.1 Synthesis of barium ferrite.....	18
2.1.1 Nickel substitution.....	19
2.1.2 Nickel -titanium substitution.....	20
2.2 Sample characterization.....	20
2.2.1 X-Ray Diffraction (XRD).....	20
2.2.2 Magnetic measurements.....	21
2.2.3 Mossbauer spectroscopy.....	22
3. RESULTS AND DISCUSSIONS.....	23
3.1 Nickel substituted ferrites.....	23
3.1.1 X-ray analysis.....	23
3.1.2 Magnetic measurements.....	24
3.1.3 Mossbauer spectroscopic analysis.....	37
3.2 Nickel-titanium substituted ferrites	47
3.2.1 X-ray analysis.....	47
3.2.2 Magnetic measurements.....	48
3.2.3 Mossbauer spectroscopic analysis.....	56
3.2 Microstructure and general discussion.....	66
4. CONCLUSIONS.....	73
REFERENCES.....	74

LIST OF FIGURES

1. Two approaches for suppressing circular magnetization effects for perpendicular and longitudinal high density recording.....4
2. Switching field distribution5
3. Unit cell of $\text{BaFe}_{12}\text{O}_{19}$ showing the polyhedra co-ordination for iron in f_{iv} and f_{vi} sites. The common faces of two polyhedra are hatched.....13
4. The closed packed layer sequence with location of iron ions in the $\text{BaFe}_{12}\text{O}_{19}$14
5. XRD pattern of pure barium ferrite $\text{BaFe}_{12}\text{O}_{19}$ (a) before and (b) after calcination.....25
6. XRD Pattern of barium hexa-ferrite of composition $\text{BaFe}_{12-x}\text{Ni}_x\text{O}_{19-x/2}$ with $x=0, 0.2, 0.4, 0.6$, and 0.826
7. XRD Pattern of barium hexa-ferrite of composition $\text{BaFe}_{12-x}\text{Ni}_x\text{O}_{19-x/2}$ with $x=0, 1.0, 1.2, 1.4$ and 1.627
8. Magnetization versus applied field curve for nickel substituted barium ferrite $\text{BaFe}_{12-x}\text{Ni}_x\text{O}_{19-x/2}$ ($x = 0, 0.2, 0.6, 1.0, 1.2, 1.4$ and 1.6).....38
9. Variation of saturation magnetization for $\text{BaFe}_{12-x}\text{Ni}_x\text{O}_{19-x/2}$ ($x = 0, 0.2, 0.6, 1.0, 1.2$ and 1.6 with amount of substitution39
10. Variation of coercivity for $\text{BaFe}_{12-x}\text{Ni}_x\text{O}_{19-x/2}$ ($x = 0, 0.2, 0.6, 1.0, 1.2, 1.4$ and 1.6) with amount of substitution39

11. Variation of magnetization with temperature barium ferrite of composition $\text{BaFe}_{12-x}\text{Ni}_x\text{O}_{19-x/2}$ ($x = 0$ and 0.6).....	40
12. Variation of magnetization with temperature barium ferrite of composition $\text{BaFe}_{12-x}\text{Ni}_x\text{O}_{19-x/2}$ ($x = 1.2$ and 1.4).....	41
13. Mossbauer spectra of barium ferrite of composition $\text{BaFe}_{12-x}\text{Ni}_x\text{O}_{19-x/2}$ ($x = 0, 0.2, 0.4$).....	43
14. Mossbauer spectra of barium ferrite of composition $\text{BaFe}_{12-x}\text{Ni}_x\text{O}_{19-x/2}$ ($x = 0.6, 0.8, 1.0$).....	44
15. Mossbauer spectra of barium ferrite of composition $\text{BaFe}_{12-x}\text{Ni}_x\text{O}_{19-x/2}$ ($x = 1.2, 1.4, 1.6$).....	45
16. Variation of hyperfine fields of different sites with nickel contents in $\text{BaFe}_{12-x}\text{Ni}_x\text{O}_{19-x/2}$ ($x = 0, 0.2, 0.4, 0.6, 0.8, 1.0, 1.2, 1.4, 1.6$).....	46
17. Variation of sextet area of different sites with nickel contents in $\text{BaFe}_{12-x}\text{Ni}_x\text{O}_{19-x/2}$ ($x = 0, 0.2, 0.4, 0.6, 0.8, 1.0, 1.2, 1.4, 1.6$).....	46
18. XRD pattern of barium ferrite of composition $\text{BaFe}_{12-2x}\text{Ni}_x\text{Ti}_x\text{O}_{19}$ ($x = 0, 0.2, 0.4, 0.6$).....	49
19. XRD pattern of barium ferrite of composition $\text{BaFe}_{12-2x}\text{Ni}_x\text{Ti}_x\text{O}_{19}$ ($x = 0.8$ and 1.0).....	50
20. Magnetization versus applied field curve for nickel and titanium substituted barium ferrite $\text{BaFe}_{12-2x}\text{Ni}_x\text{Ti}_x\text{O}_{19}$ ($x = 0, 0.2, 0.4, 0.6, 0.8, 1.0$).....	57

21. Saturation magnetization for $\text{BaFe}_{12-2x}\text{Ni}_x\text{Ti}_x\text{O}_{19}$ as a function of substitution x (x = 0, 0.2, 0.4, 0.6, 0.8, 1.0).....	58
22. Coercivity for $\text{BaFe}_{12-2x}\text{Ni}_x\text{Ti}_x\text{O}_{19}$ as function of x (x = 0, 0.2, 0.4, 0.6, 0.8, 1.0).....	58
23. Variation of magnetization with temperature for composition $\text{BaFe}_{12-2x}\text{Ni}_x\text{Ti}_x\text{O}_{19}$ with x = 0.2 and 1.0).....	59
24. Mossbauer spectra of barium ferrite of composition $\text{BaFe}_{12-2x}\text{Ni}_x\text{Ti}_x\text{O}_{19}$ (x = 0, 0.2, 0.4).....	60
25. Mossbauer spectra of barium ferrite of composition $\text{BaFe}_{12-2x}\text{Ni}_x\text{Ti}_x\text{O}_{19}$ (x = 0.6, 0.8, 1.0).....	61
26. Variation of hyperfine fields of different sites with nickel content in $\text{BaFe}_{12-x}\text{Co}_x\text{Ti}_x\text{O}_{19}$ (x=0, 0.2, 0.4, 0.6, 0.8, 1.0).....	64
27. Variation of sextet area of different sites with nickel content in $\text{BaFe}_{12-x}\text{Ni}_x\text{Ti}_x\text{O}_{19}$ (x=0, 0.2, 0.4, 0.6, 0.8, 1.0).....	64
28. Scanning electron micrographs of (a) $\text{BaFe}_{12}\text{O}_{19}$, (b) $\text{BaFe}_{12-x}\text{Ni}_x\text{O}_{19-x/2}$ with x=1.2 and (c) $\text{BaFe}_{12-2x}\text{Ni}_x\text{Ti}_x\text{O}_{19}$ with x=1.2 compounds.....	67

TABLES

1. Parameters for longitudinal and perpendicular recording.....	3
2. Key properties of magnetic materials.....	10
3. Atomic positions in hexagonal unit cell of $\text{BaFe}_{12}\text{O}_{19}$	12
4. Iron ions configuration, number per formula unit, block location and spin direction in barium ferrite $\text{BaFe}_{12}\text{O}_{19}$	12
5. Co-ordination number and direction of magnetic moment of Fe^{3+} ions in unit cell of magneto-plumbite structure.....	15
6. List of raw materials used with make and grade.....	19
7. 2θ 's, interplaner spacings and intensities of various peaks observed in XRD of nickel substituted barium ferrite composition $\text{BaFe}_{12-x}\text{Ni}_x\text{O}_{19-x/2}$ ($x=0.2$).....	28
8. 2θ 's, interplaner spacings and intensities of various peaks observed in XRD of nickel substituted barium ferrite composition $\text{BaFe}_{12-x}\text{Ni}_x\text{O}_{19-x/2}$ ($x=0.4$).....	29
9. 2θ 's, interplaner spacings and intensities of various peaks observed in XRD of nickel substituted barium ferrite composition $\text{BaFe}_{12-x}\text{Ni}_x\text{O}_{19-x/2}$ ($x=0.6$).....	30
10. 2θ 's, interplaner spacings and intensities of various peaks observed in XRD of nickel substituted barium ferrite composition $\text{BaFe}_{12-x}\text{Ni}_x\text{O}_{19-x/2}$ ($x=0.8$).....	31
11. 2θ 's, interplaner spacings and intensities of various peaks observed in XRD of nickel substituted barium ferrite composition $\text{BaFe}_{12-x}\text{Ni}_x\text{O}_{19-x/2}$ ($x=1.0$).....	32
12. 2θ 's, interplaner spacings and intensities of various peaks observed in XRD of nickel substituted barium ferrite composition $\text{BaFe}_{12-x}\text{Ni}_x\text{O}_{19-x/2}$ ($x=1.2$).....	33

13. 2θ 's, interplaner spacings and intensities of various peaks observed in XRD of nickel substituted barium ferrite composition $\text{BaFe}_{12-x}\text{Ni}_x\text{O}_{19-x/2}$ ($x=1.4$).....	34
14. 2θ 's, interplaner spacings and intensities of various peaks observed in XRD of nickel substituted barium ferrite composition $\text{BaFe}_{12-x}\text{Ni}_x\text{O}_{19-x/2}$ ($x=1.6$).....	35
15. 2θ 's, interplaner spacings and intensities of various peaks observed in XRD of standard NiFe_2O_4 and standard $\text{BaFe}_{12}\text{O}_{19}$	36
16. Saturation magnetization and coercivity of different nickel containing barium ferrite $\text{BaFe}_{12-x}\text{Ni}_x\text{O}_{19-x/2}$	37
17. Relative spectral areas and hyperfine (Internal magnetic) fields of different crystallographic sites of barium ferrite of composition $\text{BaFe}_{12-x}\text{Ni}_x\text{O}_{19-x/2}$	47
18. 2θ 's, interplaner spacings and intensities of various peaks observed XRD of nickel and titanium substituted barium ferrite of composition $\text{BaFe}_{12-2x}\text{Ni}_x\text{Ti}_x\text{O}_{19}$ ($x=0.2$).....	51
19. 2θ 's, interplaner spacings and intensities of various peaks observed XRD of nickel and titanium substituted barium ferrite of composition $\text{BaFe}_{12-2x}\text{Ni}_x\text{Ti}_x\text{O}_{19}$ ($x=0.4$).....	52
20. 2θ 's, interplaner spacings and intensities of various peaks observed XRD of nickel and titanium substituted barium ferrite of composition $\text{BaFe}_{12-2x}\text{Ni}_x\text{Ti}_x\text{O}_{19}$ ($x=0.6$).....	53
21. 2θ 's, interplaner spacings and intensities of various peaks observed XRD of nickel and titanium substituted barium ferrite of composition $\text{BaFe}_{12-2x}\text{Ni}_x\text{Ti}_x\text{O}_{19}$ ($x=0.8$).....	54

22. 2θ 's, interplaner spacings and intensities of various peaks observed XRD of nickel and titanium substituted barium ferrite of composition $\text{BaFe}_{12-2x}\text{Ni}_x\text{Ti}_x\text{O}_{19}$ ($x=1.0$).....	55
23. Saturation magnetization and coercivity of different nickel and titanium containing barium ferrite $\text{BaFe}_{12-2x}\text{Ni}_x\text{Ti}_x\text{O}_{19}$	56
24. Relative spectral areas and hyperfine (Internal magnetic) fields of different crystallographic sites of nickel and titanium containing barium ferrite $\text{BaFe}_{12-2x}\text{Ni}_x\text{Ti}_x\text{O}_{19}$	62
25. Comparison of magnetic properties of nickel and cobalt substituted barium hexaferrites.....	68
26. Comparison of magnetic properties of nickel-titanium and cobalt-titanium substituted barium hexaferrites.....	69

CHAPTER 1

INTRODUCTION

Magnetic recording involves an extremely important technology and is responsible for the widespread and relatively inexpensive use of sound and video images. Also, in conjunction with semiconductor technology, it has contributed significantly to the growth of computer development [1]. The areal density of magnetic recording in hard disk drives is increasing at an alarming rate of $\sim 60\%$ annually. The extremely high density of 10 Gbit/inch^2 is expected to be achieved in the current year itself. However, when the density level reaches near 40 Gbit/inch^2 , the thermal instability of magnetization might also occur.

In magnetic recording there is an electromagnetic transducer which converts electrical signal into magnetic fields and, in turn, magnetizes the medium. The transducer consists of a small coil (through which current passes to produce magnetic field) and the gapped magnetic structure (to intensify and localize the resulting magnetic field). The medium consists of a magnetic material coated onto a tape, disk or cylinder and moves relative to the head in close proximity by maintaining a small gap. The head field magnetizes the medium species according to the current in the coil such that time varying electrical signal gets converted into spatially varying magnetic pattern along a track. Reversal of the current causes flip over and produces transition between the regions of opposite magnetization. The read back process involves movement of medium (e.g., the tape) once again over the head. Now, the field of magnetized

region gives rise to a flux in the head coil and consequently the corresponding voltage gets induced. This way spatially varying magnetic pattern is converted back into a time varying electrical signal [2].

The fundamental problem lies in determining the optimum combination of tape, head and system parameters to meet the requirements of information super highway (e.g., multimedia). It must be of low cost and have fast access with wide transfer bandwidth. Most of these attributes can be provided by a linear system with servo-controlled multi-track arrays of integrated thin film-write/MR read heads. Currently, the concentration is primarily on advanced metallic particles and barium ferrite particulate tapes [3]. Particulate barium ferrite is a leading candidate for tapes and disks as its product gives amplitudes at recording densities of current interest that exceeds those of advanced acicular oxides and are compared to those of many commercially available media made with metallic particles (MP). The very high coercivity value of barium ferrite makes it an attractive material for future application with recording density above 100 kfc i [4]. Therefore, in the present study, we have synthesized barium ferrite by a novel auto-ignition method and tried to engineer its properties by partial substitution of iron with nickel alone and nickel-titanium together so as to meet the requirements of magnetic recording media.

1.1 Types of recording

The recording is termed as perpendicular, transverse and longitudinal depending upon the magnetization caused along the media thickness, across the media at right angles to and in the direction of

motion. In high density recording, on increasing the current, the magnetization occurs in a way that flux tends to close by itself inside the medium – a phenomenon called circular magnetization [5]. Consequently, the flux available for reproduction gets substantially reduced. Therefore, circular magnetization effect needs to be suppressed, if high-density recording is to be realized in practice. To accomplish this, one way is to make media extremely thin (e.g., magnetic thin films) so that the magnetization has large longitudinal component lying in the media plane itself. But, media then begins to exhibit strong shape anisotropy. Another way is to force magnetization in the direction normal to the media plane so that the flux closure gets inhibited and magnetization transition becomes sharp [6]. Table 1 gives the optimum parameters for high-density longitudinal and perpendicular recording. The two approaches that can suppress circular magnetization effects are shown schematically with examples in Fig. 1.

Table1: Media optimization requirement for high-density longitudinal and perpendicular recording.

Parameter	Longitudinal Recording	Perpendicular Recording
Magnetization(M_s)	Low	High Increase in M_s amounts to strong output signal with D_{50} remaining essentially same.
Coercivity (H_c)	Low	Intermediate Increase in H_c develops strong output signal at low densities only and reduces D_{50}
Thickness	Low	Intermediate
Head Coupling	Very weak	Very Strong
Interaction Between bits	Repulsive	Attractive

D_{50} is the performance parameter and refers to bit density at which output signal decrease to half of its low-density value.

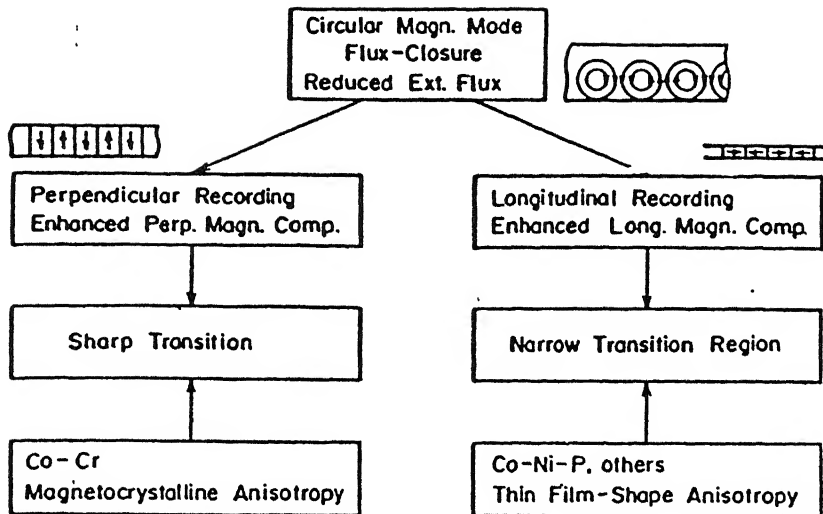


Fig. 1 : Two approaches for suppressing circular magnetization effects for perpendicular and longitudinal high density recording.

1.2 Requirements of recording medium

The retained magnetization intensity or retentivity of the medium determines the strength of the magnetic field sensed by the read back process. It is actually a measure of the magneto-motive force available to produce the signal, i.e., large retentivity produces strong output signal and therefore materials possessing such a characteristic are preferred.

The second property relates to the field strength needed to cause magnetic reversal in the media and is determined by coercivity (H_c). Its value should not be large so as to prevent successful writing and possibly overwriting or erasure by available heads, but, should be enough to resist undesirable changes or degradation of signal caused by internal or self-demagnetizing field (being proportional to magnetization intensity of media itself) during storage. So, coercivity needs to be high in strongly magnetizable coatings.

The third property is the breadth of dM/dH vs. H curve, i.e., switching field distribution (SFD) (Fig. 2). The magnetic transition is termed as sharp and well defined when SFD is narrow. Such a distribution means that the material has capacity to record information at high densities. A broad SFD corresponds to a diffuse transition and is indicative of adverse effects such as erasure, overwriting, etc. The appropriate SFD is important in systems requiring thorough erasure of information using special heads (e.g., analog recording) and in others where some residual overwritten signal can be tolerated but no erase head is used (e.g., digital recording case).

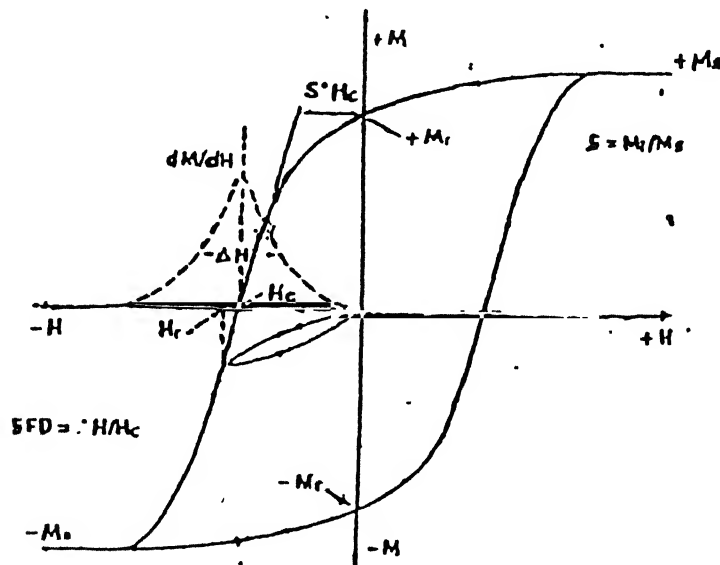


Fig.2 : Switching field distribution (dM/dH vs. H) curve .

Temperature, relative humidity and atmospheric pollutants cause deterioration in the magnetic properties of recording media, e.g., irreversible magnetic transition occurs in recording media at elevated temperature, strong temperature dependence of coercivity can endanger signal stability and also create difficulties during adjustments of writing and erasing head fields, etc. Recording data at a different temperature

critically affects the overwriting capability. Internally generated heat by motors and other components causes operational difficulties in digital equipment (e.g., disk drive, etc). Curie temperature (T_c) of recording media must be at least 50°C more than the temperature prevailing during use, transportation or storage to avoid effects of ferromagnetic-paramagnetic transition [1].

The recording media must contain small discrete rigidly placed magnetic units which remain independent (partially at least) of each other to ensure stable transition between different directions of magnetization in the recorded pattern. Each magnetized segment in the written record must contain enough sub-units to make signal-to-noise ratio adequate/high. The signal-to-noise ratio is proportional to \sqrt{n} , where n is the density of particles present (i.e., number per cm^3). Therefore, for a good recording media, particles density must be high. Also, small particle size leads to a relatively smooth surface. The effectiveness of recording and associated processes depends critically on the gap between the head and the medium. The separation (d) between the head and the medium produces another loss factor, which increases as wavelength (λ) is reduced [8]. This loss factor is proportional to $\exp(-2\pi d/\lambda)$ and in decibels corresponds to $54.6 (d/\lambda)$ [9]. Such a loss amounts to $44 (d/\lambda)$ dB and $55 (d/\lambda)$ dB during writing and reading, respectively. Further, high recording density of 50,000 bits/inch (i.e., 2000 bits/mm) corresponds to wavelength of $1\mu\text{m}$. At this density, a separation between head and tape of no more than $0.0125\mu\text{m}$ is sufficient to cause the loss of 75 percent of the available signal. Such a close spacing is difficult to achieve repeatedly particularly when recording media is removable, e.g., in case of tapes, flexible disks and some rigid disks. Recording performance is always

improved by reducing the head-medium spacing. But, this increases possibility of “head crash” or mutually destructive contact between head and medium. So, a balance must exist between recording performance on one hand and ease of media interchange, durability and longevity on the other. Surface of the medium must also be finished appropriately. The best surface is not necessarily smoothest since important functional factor of durability, friction and stiction are usually optimal when the surface of medium is not mirror like [8]. The material preparation process for recording media invariably yields a distribution of particle size. Although signal-to-noise ratio is improved by reducing the average particle size, yet, there is increasing possibility that sizeable number or portion turning super-paramagnetic - not at all useful for magnetic recording [9]. We need particles to be small enough (so as to correspond to density of $\sim 10^{14} - 10^{15}$ per cm^3), but, not so much to become unstable magnetically.

1.3 Materials for magnetic recording

Tape is considered to be appropriate for high-density recording. Existing tapes can be classified into four categories depending upon the media materials, 1) traditional $\gamma\text{-Fe}_2\text{O}_3$, 2) CrO_2 and Co-doped Fe_2O_3 , 3) metal particles (MP), and 4) doped barium ferrite (BF) particulate.

Among various oxides, $\gamma\text{-Fe}_2\text{O}_3$ turned out to the most useful material for magnetic recording because of its high chemical and physical stability. The particles in use are of acicular shape, contributing significantly to the anisotropy. Also, the magneto-static energy is minimum when the direction of magnetization and the particle longest dimension become collinear. Further, magnetic anisotropy in $\gamma\text{-Fe}_2\text{O}_3$ arises from the

interaction of electron spins with its crystal structure. The above two anisotropy determine the field needed to switch the magnetization from one energetically preferred direction to another and, in turn, coercivity [10]. $\gamma\text{-Fe}_2\text{O}_3$ particles have typical saturation magnetization density of about 340 emu/cm^3 and coercivity of 300-400 Oe and have found a number of applications not requiring high recording density [1].

The objective of achieving high coercivity material was first tried with the introduction of chromium dioxide (CrO_2) particles. Iridium doped CrO_2 particles exhibit coercivity of 500-600 Oe, magnetization intensities of $350\text{-}400 \text{ emu/cm}^3$ and a low Curie temperature of 125°C , but, are 3-4 times costly to $\gamma\text{-Fe}_2\text{O}_3$. Also, the production process for CrO_2 requires high pressures. Moreover, CrO_2 particles are quite abrasive and somewhat reactive [11]. Audio, video and data disks, however, require materials of high coercivity (1000-2500Oe). The magneto-crystalline anisotropy constant gets tripled with increase in coercivity when 4% of iron is substituted with cobalt in $\gamma\text{-Fe}_2\text{O}_3$. But, in the process the particles assume almost spherical shape with reduction in acicularity. Also, the coercivity then becomes sensitive to temperature and pressure. A magnetic particle developed with trade name AVILYN exhibits high coercivity is an acicular iron oxide with some cobalt compounds dispersed on the surface. The coercivity of the particles is controllable in the range 450–800 Oe. These particles display much improved thermal stability with regard to coercivity [12].

The metal particles (MP) have a range of choice of magnetization and coercivity, e.g., pure iron has a high saturation magnetization of 1700 emu/cm^3 . Also, the coercivity of acicular iron particles is about 2-5 times

higher than that of $\gamma\text{-Fe}_2\text{O}_3$ particles of the same shape. Iron particles of coercivity 1100-1700 Oe are now commercially available too. However, metal particles are usually susceptible and tend to corrode in atmosphere and react with binders [3]. The particles having a coercivity of ~ 1000 Oe exhibit high signal-to-noise ratio and so found applications in audio and 8 mm video tapes. On the other hand, particles having a coercivity of ~ 1500 Oe are useful for high-density flexible disks [13].

The key properties of different magnetic materials used for recording are summarized in Table 2. Among these only metal particle and barium ferrite are of current interest for ultrahigh density magnetic recording. Though metallic particles are popular, barium ferrite is of current interest for ultrahigh density recording [8].

Barium hexa-ferrite media has immense potential application in high-density recording largely due to its specific direction of magnetization. The platelets are forced (by strong magnetic field applied) to lie with their planer surface parallel to the substrate. The direction of magnetization is then normal to the substrate and configuration makes pure $\text{BaFe}_{12}\text{O}_{19}$ ideal for perpendicular recording. Also, it is chemically very stable, exhibits excellent oxidation/corrosion resistance, and can be synthesized with existing low cost mass production facilities. The platelet shaped particles can be produced with well-defined size range, shape uniformity and morphological perfection. Besides, coercivity can be controlled over a wide range to suit variety of applications. But, there are some associating problems too, mainly due to competing orthogonal anisotropies (crystalline and shape) of the platelet-shaped particles, temperature dependence of magnetic parameters, e.g., coercivity [1].

Table 2: Key properties of magnetic materials.

Particle Property	$\gamma\text{-Fe}_2\text{O}_3$	$\text{Co-Fe}_2\text{O}_3$	CrO_2	$\text{Ba}_{0.6}\text{Fe}_{2.03} + \text{Co, Ti}$	Fe	Fe_4N
σ_s saturation magnetization, emu/g	73-74	73-76.3	70-80	45-70	150-190	110-130
$\frac{\sigma_r}{\sigma_s}$	0.5	0.5-0.8	0.5	0.6-0.7	0.23-0.52	0.47-0.53
Curie Temperature, T_c , °C	[590]	[590]	115-126	320	768	490
magnetocrystalline anisotropy constant, K_1 , ergs/cc	-4.64×10^4	$-5 r_0 + 100 \times 10^4$	$+2.5 \times 10^5$	$+3.3 \times 10^6$	$+4.4 \times 10^5$	
saturation magnetostriction λ_s	-5×10^{-6}	-5 to -15×10^{-6}	$+1 \times 10^{-6}$		$+4 \times 10^{-6}$	
coercivity, H_c , Oe	250-350	550-750	450-670	320-1970	375-1650	640-1100
switching field distribution, $\frac{\Delta H}{H_c}$	0.26-0.61	0.30-0.6	0.35-0.6	0.16-0.6	0.5-0.75	0.5-0.7
temperature coeff. of coercivity, $\Delta H_c/H_c/^\circ\text{C}$ (20-70°C)	-1×10^{-3}	impreg. ^d -2.4×10^{-3} doped -10×10^{-3}	-5×10^{-3}	$+3.1 \times 10^{-3}$	-0.6×10^{-3}	-0.7×10^{-3}
specific surface area (BET), m^2/g	20-40	20-40	25-37	15-31	26	25-40
density, ρ , g/cc	4.60	4.80	4.88-4.95	5.28	5.8	5.8
crystal structure	cubic $a_0 = 25 \text{ \AA}$, m3m	cubic	tetragonal $a = 4.4218 \text{ \AA}$ $c = 2.9182 \text{ \AA}$	hexagonal $c = 23.2 \text{ \AA}$ $a = 5.88 \text{ \AA}$	b.c.c. $a = 2.861 \text{ \AA}$	f.c.c. $a = 3.795 \text{ \AA}$
ferro- or ferrimagnetic	ferr	ferr	ferro	ferr	ferro	ferro
particle size, μm	needles $l = 0.3$ $d = 0.06$	needles equi ax. $l = 0.3$ $l = 0.2$ $d = 0.06$	needles $l = 0.5$ $d = 0.05$	hex. platelets $\text{dia} = 0.08-0.1$ $\text{thick} = 0.01-0.025$	needles $l = 0.3$ $d = 0.06$	$l = 0.5$ $\text{dia} = 0.07$

1.4 Barium ferrite

The barium ferrite ($\text{BaFe}_{12}\text{O}_{19}$) has a magneto-plumbite structure with hexagonal unit cell having parameter $a = 5.892 \text{ \AA}$, $c = 23.183 \text{ \AA}$, $Z = 2$ and space group $p6_3/mmc$ [14]. The unit cell contains two formula units of $\text{BaFe}_{12}\text{O}_{19}$ and consists of S and R blocks in sequence of RSR^*S^* , where asterisks indicate a 180° rotation with respect to c-axis (Fig. 3). The R block in this case is formed by the group $(\text{BaFe}_6\text{O}_{11})^{2-}$ whereas S block comprises of $(\text{FeO}_8)^{2+}$ and has no barium cation. The O^{2-} layer containing Ba^{2+} is a mirror plane, being perpendicular to the c-axis. The

oxygen has a cubic close packing configuration (i.e., ABCABC...) in the S block and hexagonal layer sequence (i.e., ABAB..) in the R block. The [111] cubic axis coincides with the [0001] hexagonal axis. Fe^{3+} ions occupy interstitial position in oxygen layers in five different crystal sites (viz., k, f_{vi} , a, f_{iv} and b). There are 12 octahedral 'k'-sites, four tetrahedral ' f_{iv} ' sites (or f_1), four octahedral ' f_{vi} ' sites (or f_2), two octahedral 'a' sites, and two 'b' five-fold sites (Fig. 3). R and S units share the twelve iron ions of the k-sites. The four Fe^{3+} ions in f_{vi} locations are in R block close to Ba^{2+} ions and forming a Fe_2O_9 group of two octahedra with a common face. Two Fe^{3+} ions in 'a' sites are present in S block. The two 'b' sites with five-fold symmetry are formed by two tetrahedra sharing a common face. A detailed XRD study has shown that Fe^{3+} ions lie in a double potential well of the trigonal bipyramid [15]. Table 3 gives the atomic positions of the hexagonal unit cell of $\text{BaFe}_{12}\text{O}_{19}$. Fig. 4 shows the unit cell together with layer sequence and distribution of various species. The Fe^{3+} ions configuration, number per formula unit, block location and spin direction in the $\text{BaFe}_{12}\text{O}_{19}$ are given in Table 4 [13].

Barium ferrite unit cell contains twenty-four Fe^{3+} ions, each with moment of $5\mu_B$ (Bohr magneton). Their moments lie perpendicular to close packed oxygen layers, i.e., parallel or antiparallel to c-axis or [0001]. By assuming the known spin directions of Fe^{3+} ions in spinel structure (or S block) and applying the principles governing the super exchange force, one can proceed from ion to ion throughout the cell and predict the direction of its net spin moment, i.e., parallel or antiparallel to [0001]. Coordination number and direction of magnetic moment of Fe^{3+} ions in unit cell of magneto-plumbite structure are shown in Table 5. This suggests spins of 16 ions in one direction and of 8 in the other (since unit

cell contains two formula units of $\text{BaFe}_{12}\text{O}_{19}$). The net magnetic moment should therefore be $(16-8) \times 5 \mu_B = 40 \mu_B$ per cell or $20 \mu_B$ per molecule of $\text{BaFe}_{12}\text{O}_{19}$. This corresponds to 100 emu/g and agrees well with the measured value of the saturation magnetization at 0K [16].

Table 3 : Atomic positions in hexagonal unit cell of $\text{BaFe}_{12}\text{O}_{19}$

Ion	Site	Co-ordinates	x	z
2Ba^{2+}	2d	$1/3, 2/3, 3/4 ; 2/3, 1/3, 1/4$	-	-
	2a	$0, 0, 0 ; 0, 0, 1/2$	-	-
	2b	$0, 0, 1/4 ; 0, 0, 3/4$	-	-
24Fe^{3+}	$4f_1$	$\pm(1/3, 2/3, z ; 2/3, 1/3, 1/2 + z)$	-	0.028
	$4f_2$	$\pm(1/3, 2/3, z ; 2/3, 1/3, 1/2 + z)$	-	0.189
	12k	$\pm(x, 2x, z ; 2x, x, z ; x, x, z ; x, 2x, 1/2 - z ; 2x, x, 1/2 + z ; x, x, 1/2 + z)$	0.167	- 0.108
38O^{2-}	4e	$\pm(0, 0, z ; 0, 0, 1/2 + z)$	-	0.150
	4f	$\pm(1/3, 2/3, z ; 2/3, 1/3, z)$	-	-0.050
	6h	$\pm(x, 2x, 1/4 ; 2x, x, 3/4 ; x, x, 1/4)$	0.186	-
		$\pm(x, 2x, z ; 2x, x, z ; x, x, z ; x, 2x, 1/2 - z ; 2x, x, 1/2 + z ; x, x, 1/2 + z)$	0.167	0.050
	12k	$\pm(x, 2x, z ; 2x, x, z ; x, x, z ; x, 2x, 1/2 - z ; 2x, x, 1/2 + z ; x, x, 1/2 + z)$	0.500	0.150

Table 4: Iron configuration; number per formula unit, block location and spin direction in pure barium ferrite of composition $\text{BaFe}_{12}\text{O}_{19}$

Site	Configuration	Number	Block	Spin
$4f_{vi}$	Octahedral	2	R	Down
2b	Bipyramidal	1	R	Up
12k	Octahedral	6	R-S	Up
$4f_{iv}$	Tetrahedral	2	S	Down
2a	Octahedral	1	S	Up

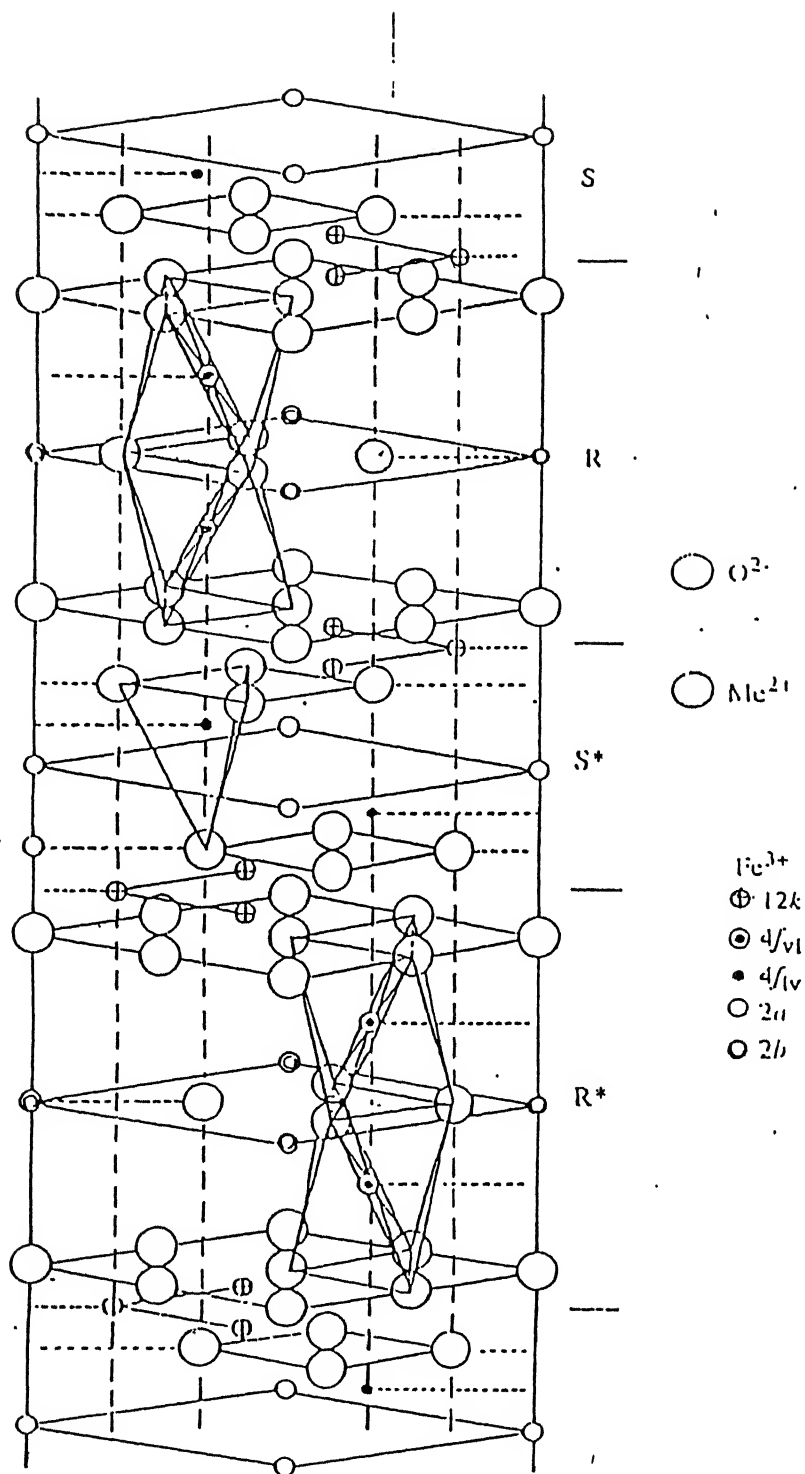


Fig. 3: Unit cell of $BaFe_{12}O_{19}$ showing polyhedral co-ordination of iron in f_{iv} and f_{vi} sites. The common faces of two polyhedra are hatched. Astrick(*) indicates a rotation of a block of the cell over 180° around the vertical c-axis.

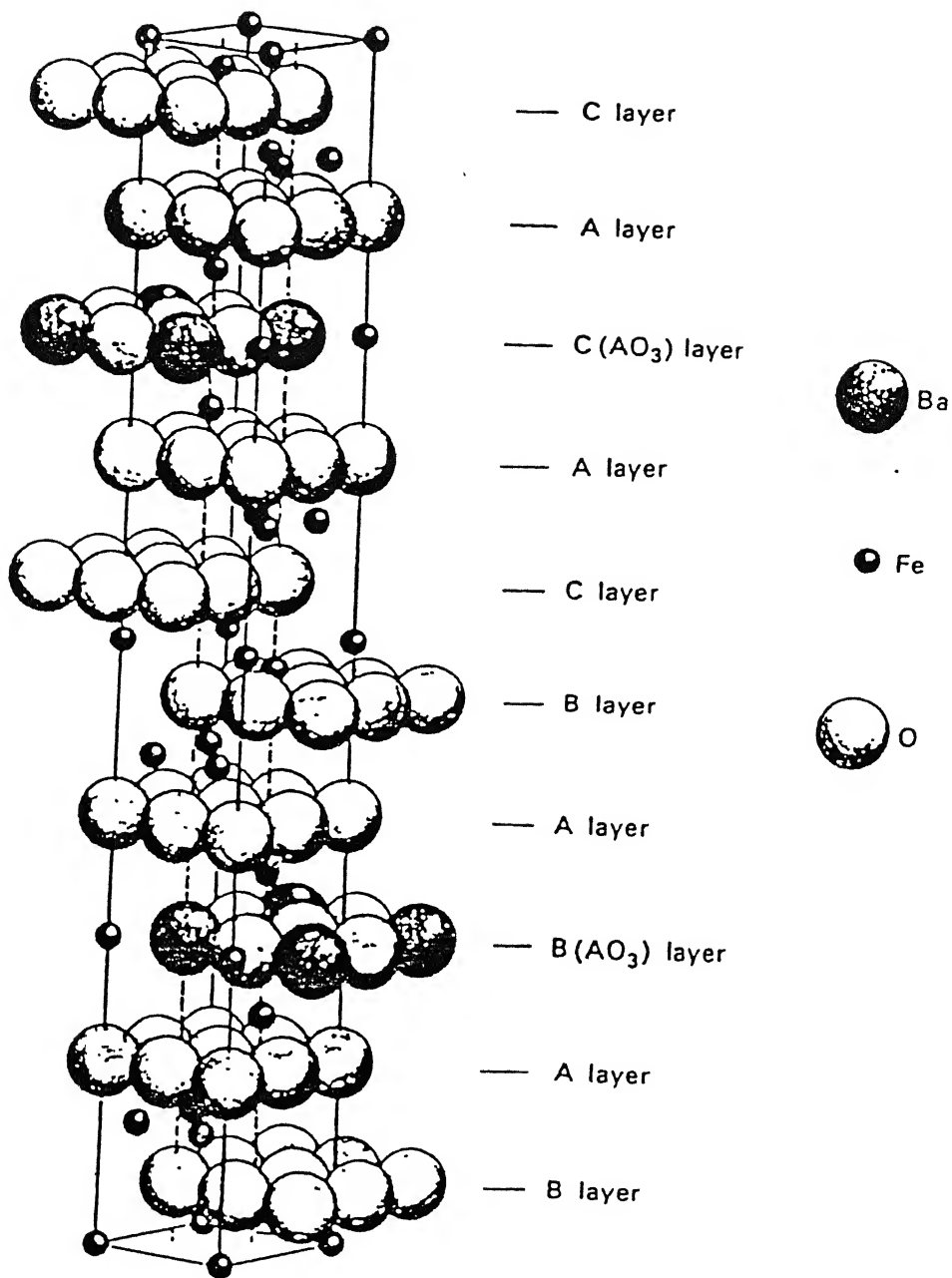


Fig. 4: The closed packed layer sequence of oxygen with location of iron ions in $\text{BaFe}_{12}\text{O}_{19}$

The Curie temperature is 450⁰ C. (1 Bohr Magnetron =9.27 x 10⁻²⁰emu and Molecular weight of BaFe₁₂O₁₉ = 1113 gm.)

Barium ferrite usually grows as platelets with their c-axis along the thickness, i.e., normal to the plane of the platelet. Such a growth habit leads to a moment arising due to shape and magneto-crystalline anisotropies perpendicular to each other. The coercivity (total anisotropy field) H_c for a random particle assembly is given by

$$H_c = C (2k/M_s - N_d M_s)$$

where M_s is the saturation magnetization, N_d is shape-demagnetizing factor considered to be unity for thin platelets, k is the magneto-crystalline anisotropy constant and C is constant [17].

Table 5 : Coordination number and direction of magnetic moment of Fe³⁺ ions in unit cell of magneto-plumbite structure.

Co-ordination Number	Number of Positions	Notation/ locations	Direction of Magnetic moment
6 (octahedral site)	12 4 2	k f _{vi} a	↑↑↑↑↑↑ ↓↓ ↑
4 (Tetrahedral site)	4	f _{iv}	↓↓
5 (Trigonal bipyramidal site)	2	b	↑

1.5 Synthesis methods

There are two major routes namely ‘particulate’ and ‘thin film’ for the synthesis of magnetic recording media. Each produces a layer of

magnetic species on the surface of a support such as plastic film (for tapes, flexible floppy disks, etc.) or aluminum plate (for rigid disks). The newer methods involves deposition of thin films of oxide, pure metal, or alloy on the support by thermal evaporation, sputtering or chemical plating. Recording media produced by thin film technology exhibit nearly ideal magnetic property. Thin film, however, pose some practical difficulties in production and so they found limited use. On the other hand, there exists infrastructure and expertise for manufacturing besides immense application experience for particulate media [18].

Ferrites can be synthesized through solid state reaction routes in wide variety of forms - polycrystalline aggregates, thin and thick films, single crystal, etc. A few other important techniques include ceramic, co-precipitation, sol-gel, glass crystallization and auto-ignition [19-25]. Of these, auto-ignition method has of late become popular because it is simple, allows reaction to occur at relatively low temperature and consumes less energy. This process essentially involves initiation of combustion of ingredients at a low temperature and makes use of the heat energy liberated by exothermic anionic oxidation. The combustion reaction is instantaneous, self-propagating and non-explosive in nature. This method produces precursor containing small amount of carbon impurities that get expelled by forming CO_2 on calcination. Thus, it cuts down a step too involving burning of the precursor [25].

1.6 Objective of the present work

The objective has been to substitute iron partially with nickel and nickel-titanium in barium ferrite and prepare compounds of compositions

$\text{BaFe}_{12-x}\text{Ni}_x\text{O}_{19-x/2}$ and $\text{BaFe}_{12-2x}\text{Ni}_x\text{Ti}_x\text{O}_{19}$ with x (in steps of 0.2) up to 1.6 and 1.0, respectively by auto-ignition method and study their phase(s), magnetic characteristics (e.g., specific magnetization, coercivity and Curie temperature) and Mossbauer spectra for developing high density media for information storage applications. For this, an attempt has been to gather information about site occupancy of Ni^{2+} and Ni^{2+} - Ti^{4+} ions in respective barium ferrites and determine factors responsible for controlling their characteristic properties.

CHAPTER 2

EXPERIMENTAL DETAILS

In this chapter, the experimental details pertaining to synthesis of pure and modified barium ferrites by partial substitution of iron with nickel and nickel-titanium and their characterization by X-ray diffraction (XRD), magnetic measurements and Mossbauer spectroscopy are given.

2.1 Synthesis of barium ferrite

The raw materials used with their make and grade are listed in Table 6. The stoichiometric amounts (ratio 1:12) of the aqueous solutions of $\text{Ba}(\text{NO}_3)_2$ and $\text{Fe}(\text{NO}_3)_3 \cdot 9\text{H}_2\text{O}$ are first mixed thoroughly. One gram mole of citric acid for each gram mole of total metal ions is then added to mixed aqueous solution and stirred magnetically at a temperature of 90°C for 20 minutes. This yields a light yellowish solution of pH around 2.0. To ensure homogeneous mixing of components, ethylene diamine is added. This raises the pH of the solution. The addition is continued till pH reaches 6.5 and heating commenced. After a while, the liquid begins to set into a gel with color changing to dark blue. On further heating, the gel starts to foam and swell. Subsequently, the dry gel catches fire on its own with appearance of glowing flints and evolution of large amount of gases of light reddish color (suspected to be NO_x type). The self-sustained spontaneous combustion process gets completed within a few minutes producing brown ash containing fine flakes. The ash is calcined at 1000°C for ten hours to yield the final product, i.e., barium hexaferrite.

Unlike other combustion processes, the autocatalytic combustion occurs here irrespective of the heating rate, stoichiometry and mass-to-volume ratio of the mixture. The process is non-explosive and so no extra care is needed to check the vigour of the reaction.

Table 6: List of raw materials used with make and grade.

Material	Make	Grade
Barium Nitrate $\text{Ba}(\text{NO}_3)_2$	Thomas baker	L.R
Ferric Nitrate $\text{Fe}(\text{NO}_3)_3 \cdot 9\text{H}_2\text{O}$	Nice	L.R
Citric acid $\text{CH}_2\text{-COOH}$ HO-C-COOH $\text{CH}_2\text{-COOH}$	International Chemical industries	A.R
Nickel nitrates $\text{Ni}(\text{NO}_3)_2 \cdot 6\text{H}_2\text{O}$	Nice	L.R
Ethylene diamine	S.D fine chemical Ltd	L.R
Titanium Oxide TiO_2	Nice	L.R

2.1.1 Nickel substitution

For synthesis of barium ferrite of composition $\text{BaFe}_{12-x}\text{Ni}_x\text{O}_{19-x/2}$ with $x=0.2, 0.4, 0.6, 0.8, 1.0, 1.2, 1.4$ and 1.6 , appropriate amounts of $\text{Ba}(\text{NO}_3)_2$, $\text{Fe}(\text{NO}_3)_3 \cdot 9\text{H}_2\text{O}$ and $\text{Ni}(\text{NO}_3)_2 \cdot 6\text{H}_2\text{O}$ were added to the required amount of citric acid. Ethylene diamine was added till the pH reached at a level of 6.5 as in the case of pure barium ferrite. The solution was then stirred properly and heated to yield ash as before. The

ash is then calcined at 1000⁰ C for 10 hours in each case to get the final product.

2.1.2 Nickel-titanium substitution

In another batch, partial substitution of iron was undertaken with nickel and titanium together to produce barium ferrite of composition $\text{BaFe}_{12-2x}\text{Ni}_x\text{Ti}_x\text{O}_{19}$ with $x = 0.2, 0.4, 0.6, 0.8$ and 1.0 . Due to non-availability of aqueous solution of Ti^{4+} , TiO_2 powder was mixed in required amount in solution of barium, nickel and iron nitrates with citric acid. Further, since TiO_2 is not soluble in water, proper mixing was ensured by high level of powder dispersion with addition of ethylene diamine. The ash formed from such a mixture was calcined at 1000⁰ C for 10 hours to get the final product.

2.2 Sample characterization

2.2.1 X-Ray diffraction (XRD)

The XRD patterns of various samples have been recorded in a Rich-Seifert X-ray diffractometer (model ISO Debye flux 2002) using $\text{CuK}\alpha$ radiation to ascertain the nature of barium ferrites and to find out the phase(s) present. For this, powder was packed in a 10mm diameter circular cavity of perspex sample holder, which was then mounted in its position on the diffractometer. The diffracted beam was received by a scintillation counter detector, held at an angle of 2θ with the transmitted beam. The X-ray tube was operated at 30kV and 20 mA and XRD pattern recorded at a scanning rate of 3°/min and a chart speed of 30 mm/min.

The time constant was 10 seconds and sensitivity was either 5000 or 2000 counts per minute.

2.2.2 Magnetic measurements

Initially, 1ml of 1% polyvinyl alcohol (binder) was added to one gram of ferrite sample and slurry formed was mixed properly in a mortar for fifteen minutes. Subsequently, the slurry was kept in an oven at 90°C for two hours and allowed to cool. A pellet of size 3mm x 3mm x 4mm was then made by using a special die, fabricated for the purpose. All the pellets were kept at 400°C for two hours so as to expel the polyvinyl alcohol present. The magnetic moment measurements were carried out with a parallel field vibrating sample magnetometer VSM (Princeton Applied Research Model -150 A) in conjunction with an electromagnet (Varian model V-2700), providing a magnetic field of up to 11.5 kOe. Also, the magnetic moments versus temperature data were obtained at a fixed magnetic field of 10 kOe to determine the Curie temperature of the products. The temperature of the sample chamber was set with a controller (Indotherm model 401) and a regulated power supply (Networks model NPS 30/5D). A chromel-alumel thermocouple was held close to the sample to indicate the temperature. The sample chamber was evacuated using a HHV pumping module during the heating process.

The information derived from the measurements at room temperature comprises of specific magnetization (M_s), remanance magnetization (M_r), and coercive field (H_c). The Curie temperature (T_c) was, however, determined for pure and some nickel and nickel-titanium modified barium ferrites.

2.2.3 Mossbauer spectroscopy

About 50mg of each sample was spread uniformly in a circular area of 12-mm diameter and sandwiched between the cello tape pieces. A vibrating radioactive source ^{57}Co of strength 5mC embedded in rhodium matrix provided γ -rays to fall on the sample. A gas filled proportional counter was used to detect the transmitted radiation. The signal generated was digitized and counts stored in a multichannel analyzer. The Mossbauer spectra were taken in a constant acceleration mode with V_{max} as ± 15 mm/s and calibrating the set-up with ^{57}Fe source. Their analyses were carried out using a computer program in FORTRAN language assuming the spectral lines to be of Lorentzian shapes and considering singlets, doublets and sextets contributions separately. The information about the parameters like isomer shifts, quadruple splitting, line width and internal hyperfine fields were obtained from the Mossbauer spectra.

CHAPTER 3

RESULTS AND DISCUSSION

3.1 Nickel substituted ferrites

3.1.1 X-ray analysis

The X-ray diffraction patterns of $\text{BaFe}_{12}\text{O}_{19}$ before and after calcination at 1000°C for 10h are shown in Fig. 5. As evident, crystalline phase developed after the calcination process only. For this reason, all subsequent samples were also calcined at 1000°C for 10h. XRD patterns for $\text{BaFe}_{12-x}\text{Ni}_x\text{O}_{19-x/2}$ with $0 \leq x \leq 1.6$ are shown in Figs. 6 and 7. The d-values and relative intensities of various diffraction peaks with their indices are given in Tables 7-14. The standard data of $\text{BaFe}_{12}\text{O}_{19}$ are also included for the sake of comparison. The indexing of patterns suggests a hexagonal structure with unit cell parameters as $a=5.867 \pm 0.001 \text{ \AA}$ and $c=23.310 \pm 0.001 \text{ \AA}$ for the entire synthesized product. This match reasonably well with known crystal data as $a=5.895 \text{ \AA}$, $c=23.215 \text{ \AA}$, $Z=2$ and space group $P6_3/\text{mmc}$ for the magneto-plumbite structure of $\text{BaFe}_{12}\text{O}_{19}$ [26]. However, as nickel substitution increases beyond $x=0.6$, the intensities of 11.0, 10.8 and 22.0 reflections increase. Moreover, these reflections become prominent for samples of composition corresponding to $x=1.4$ and $x=1.6$. Concurrently, reflections 10.7 and 11.4 become weaker. These observations suggest that the compound $\text{BaFe}_{12-x}\text{Ni}_x\text{O}_{19-x/2}$ continues to maintain magneto-plumbite structure up to $x=0.6$ at least. Also, another phase of composition NiFe_2O_4 emerges in increasing amount with rise of nickel content. Incidentally, nickel ferrite NiFe_2O_4

exhibits cubic structure (inverse spinel type) with $a=8.33$ Å, $Z=8$ and space group $Fd3m$ [27]. The oxygen ions form a cubic closed packed configuration with nickel ions in octahedral voids and iron ions uniformly distributes over the remaining octahedral and tetrahedral sites. This arrangement resembles with S block of magneto-plumbite structure. For comparison, crystal data of $NiFe_2O_4$ are also summarized with that of $BaFe_{12}O_{19}$ in Table 15. Though the XRD patterns do match reasonably well with the crystal data of $NiFe_2O_4$ and $BaFe_{12}O_{19}$ both, there is every possibility of altogether a new phase developing with different unit cell and space group, considering the close resemblance between the nickel ferrite and the barium ferrite structures. It requires further experimentation to gather more information for resolving the issue fully.

3.1.2 Magnetic Measurements

The magnetization vs. magnetic field curves of nickel substituted barium ferrites of composition with $x = 0, 0.2, 0.6, 1.0, 1.2, 1.4$ and 1.6 at room temperature are shown in Fig. 8. The values of their saturation magnetization (M_s), coercivity (H_c) and the Curie Temperature (T_c) are shown in Table 16. The M_s vs. x graph (Fig. 9) clearly reveals that the saturation magnetization decreases continuously with nickel content and assumes values of 59.3 emu/g and 43.4 emu/g for $x=0$ and 1.6 , respectively. The coercivity value also decreases continuously for all substitution and corresponds to 4300 Oe and 1379 Oe for $x=0$ and $x=1.6$, respectively (Fig. 10). These observations suggest that nickel substitution is primarily responsible for the decrease in both the saturation magnetization and coercivity values. Also, the shape of the M-H curve is changing (Fig. 8).

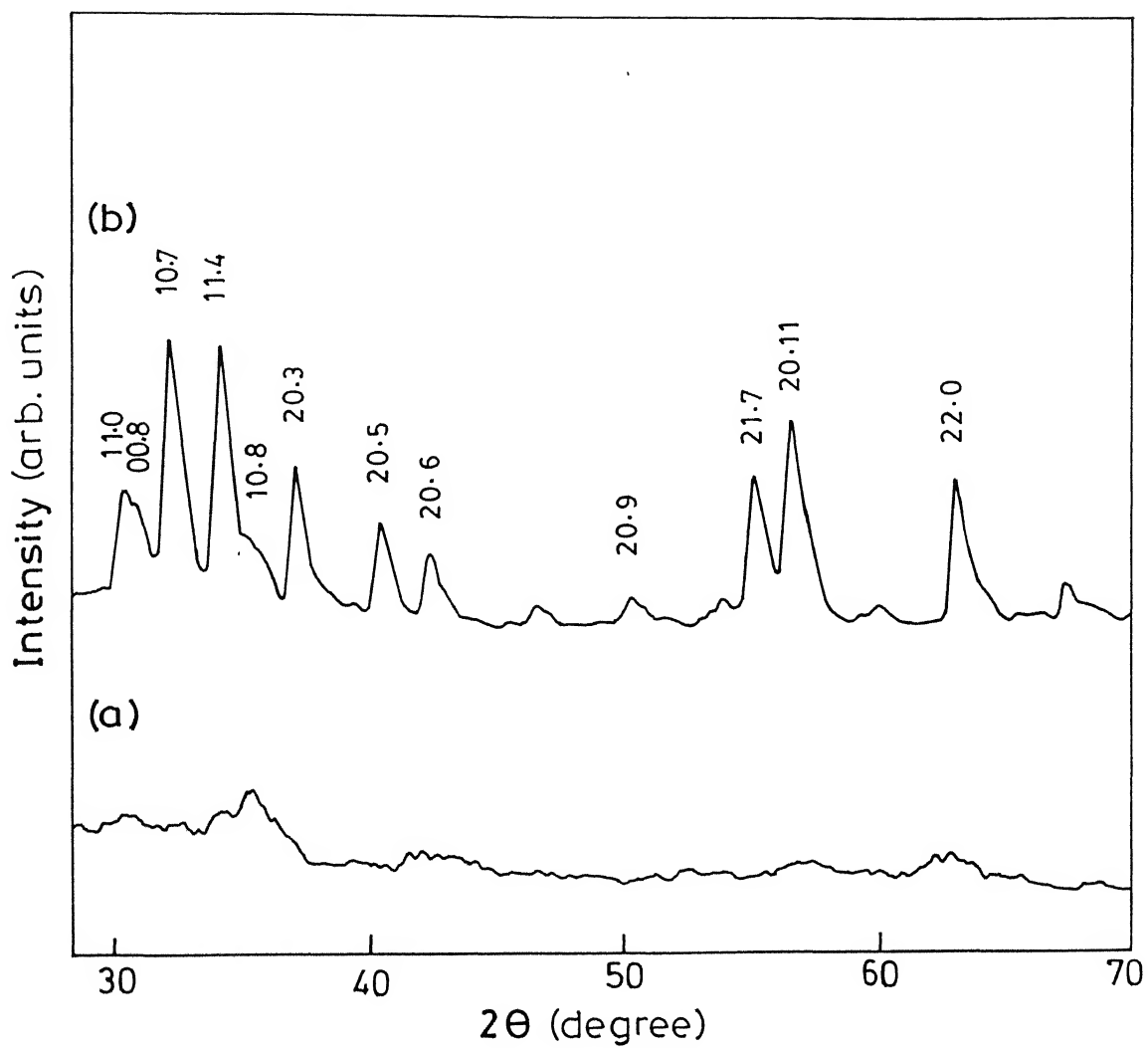


Fig 5: XRD pattern of pure barium ferrite $\text{BaFe}_{12}\text{O}_{19}$ (a) before and (b) after calcination at 1000°C for 10 hours.

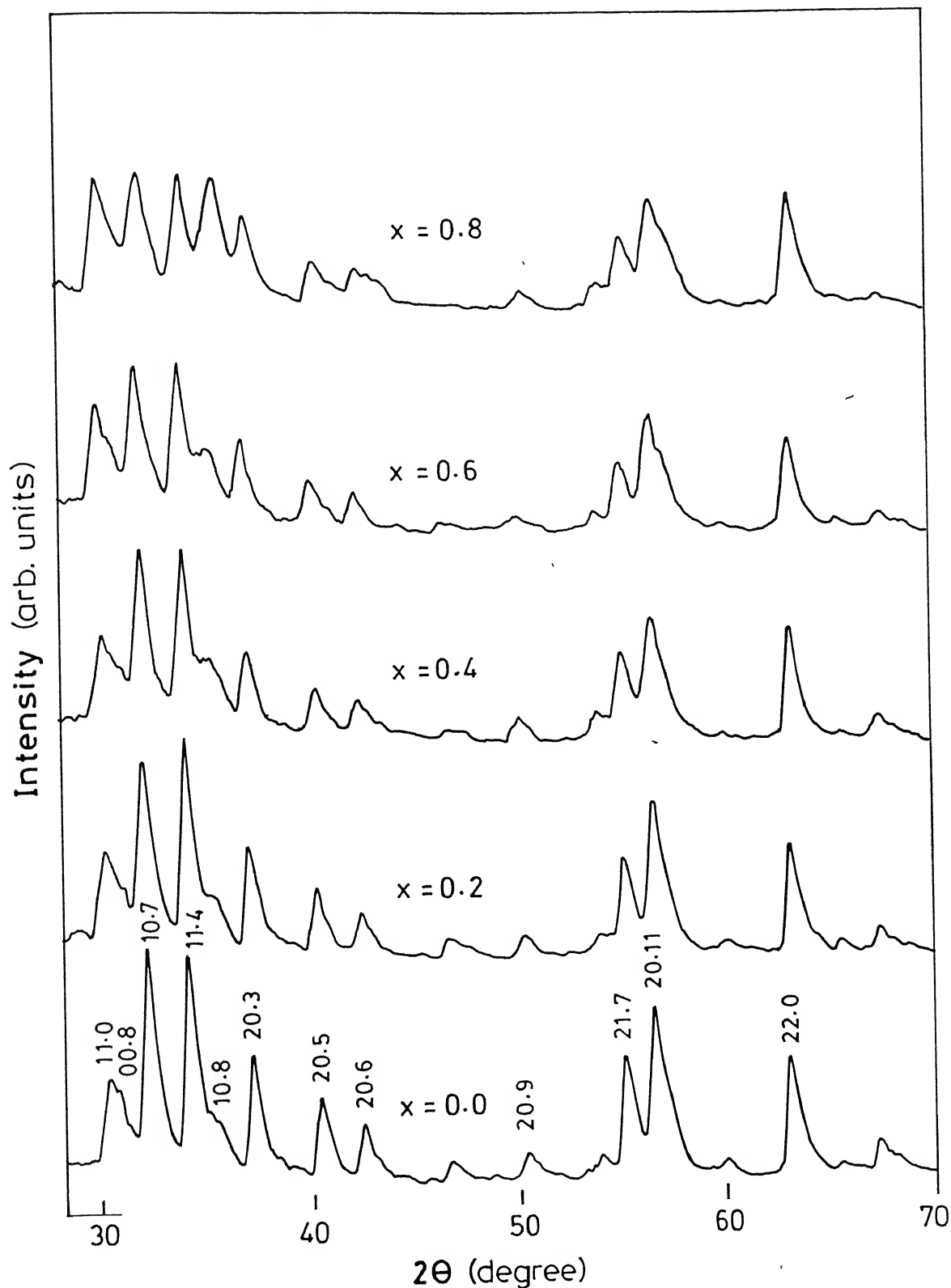


Fig 6: XRD Pattern of barium hexa-ferrite of composition $\text{BaFe}_{12-x}\text{Ni}_x\text{O}_{19-x/2}$ with $x=0, 0.2, 0.4, 0.6$ and 0.8

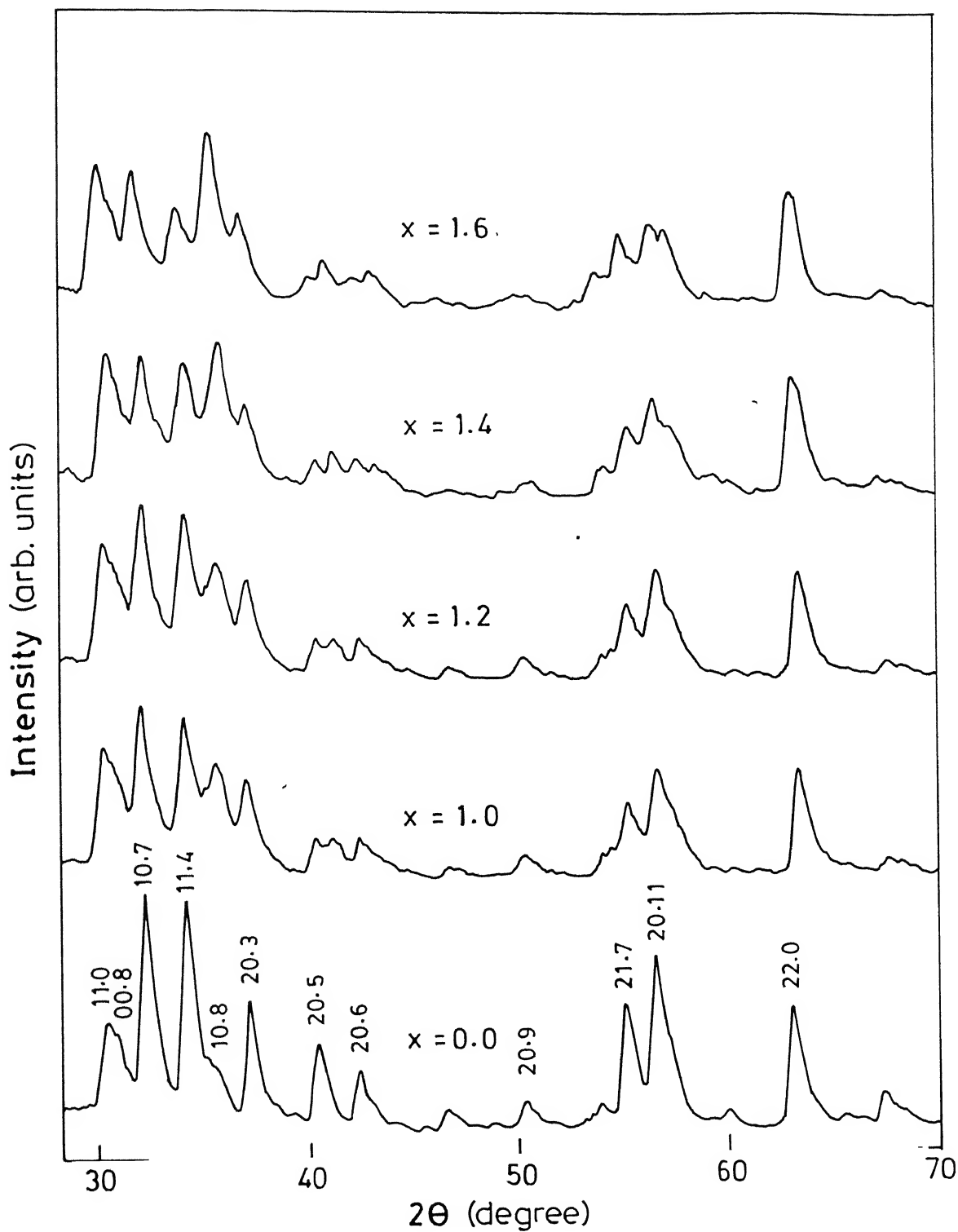


Fig . 7: XRD Pattern of barium hexa-ferrite of composition $\text{BaFe}_{12-x}\text{Ni}_x\text{O}_{19-x/2}$ with $x=0, 1.0, 1.2, 1.4$ and 1.6 .

Table 7 : 2 θ 's, interplaner spacings and intensities of various peaks observed in XRD of nickel substituted barium ferrite of composition BaFe_{12-x}Ni_xO_{19-x/2}

x=0 Standard data				x=0 Observed		x=0.2 Observed	
2 θ°	d(\AA)	Relative intensity	h k l	d(\AA)	Relative intensity	d (\AA)	Relative Intensity
22.9	3.868	18	0 0 6	3.847	8	3.880	12
30.2	2.948	55	1 1 0	2.938	40	2.947	47
30.8	2.901	32	0 0 8	2.901	36	-	-
31.3	2.859	9	1 1 2	-	-	2.864	<1
32.1	2.782	100	1 0 7	2.786	100	2.786	94
34.1	2.628	98	1 1 4	2.627	97	2.635	100
35.1	2.553	11	2 0 0	-	-	-	-
35.6	2.522	10	1 0 8	-	-	-	-
37.0	2.425	60	2 0 3	2.428	50	2.428	47
38.7	2.322	<1	0 0 10	-	-	-	-
39.1	2.303	4	1 0 9	-	-	-	-
40.3	2.237	29	2 0 5	2.231	35	2.247	34
42.4	2.131	18	2 0 6	2.130	23	2.130	18
42.8	2.113	3	1 0 10	-	-	-	-
46.4	1.949	9	1 0 11	1.947	9	1.955	10
46.9	1.934	<1	0 0 12	-	-	-	-
49.9	1.823	6	1 0 10	-	-	-	-
50.3	1.814	10	2 0 9	1.812	12	1.816	10
53.2	1.718	3	2 0 10	-	-	-	-
53.8	1.701	8	3 0 0	1.697	10	-	-
54.4	1.684	5	3 0 2	-	-	1.674	52
55.0	1.668	53	2 1 7	1.668	55	-	-
55.4	1.658	8	0 0 14	-	-	-	-
56.3	1.633	30	3 0 4	-	-	-	-
56.5	1.626	58	2 0 11	1.630	78	1.630	82
56.8	1.618	10	1 1 12	-	-	-	-
57.3	1.606	7	2 1 8	-	-	-	-
58.4	1.578	3	1 0 14	-	-	-	-
59.8	1.546	2	2 1 9	-	-	1.540	6
59.9	1.541	3	2 0 12	-	-	-	-
62.5	1.484	2	2 1 10	-	-	-	-
62.7	1.481	6	1 0 15	-	-	-	-
63.0	1.474	63	2 2 0	1.474	54	1.474	59
63.5	1.463	5	2 0 13	-	-	-	-
64.1	1.451	<1	0 0 16	-	-	-	-
65.5	1.424	3	2 1 11	-	-	1.422	<1
67.3	1.390	13	2 0 14	1.388	14	1.388	<10
68.0	1.377	4	2 2 6	-	-	-	-
71.7	1.314	9	2 2 8	-	-	1.314	<10
72.0	1.310	4	2 1 13	1.310	7	-	-
72.5	1.302	15	3 1 7	1.304	27	1.304	16
74.1	1.278	3	3 0 12	-	-	-	-
75.4	1.259	6	4 0 3	-	-	1.260	<10

Table 8 : 2θ 's, interplaner spacings and intensities of various peaks observed in XRD of nickel substituted barium ferrite of composition $\text{BaFe}_{12-x}\text{Ni}_x\text{O}_{19-x/2}$

x=0 Standard data				x=0 Observed		x=0.4 Observed	
$2\theta^\circ$	$d(\text{\AA})$	Relative intensity	h k l	$d(\text{\AA})$	Relative intensity	$d(\text{\AA})$	Relative Intensity
22.9	3.868	18	0 0 . 6	3.847	8	-	-
30.2	2.948	55	1 1 . 0	2.938	40	2.947	34
30.8	2.901	32	0 0 . 8	2.901	36	-	-
31.3	2.859	9	1 1 . 2	-	-	-	-
32.1	2.782	100	1 0 . 7	2.786	100	2.786	100
34.1	2.628	98	1 1 . 4	2.627	97	2.612	84
35.1	2.553	11	2 0 . 0	-	-	-	-
35.6	2.522	10	1 0 . 8	-	-	-	-
37.0	2.425	60	2 0 . 3	2.428	50	2.562	47
38.7	2.322	<1	0 0 . 10	-	-	-	-
39.1	2.303	4	1 0 . 9	-	-	-	-
40.3	2.237	29	2 0 . 5	2.231	35	2.241	29
42.4	2.131	18	2 0 . 6	2.130	23	2.125	21
42.8	2.113	3	1 0 . 10	-	-	-	-
46.4	1.949	9	1 0 . 11	1.947	9	-	-
46.9	1.934	<1	0 0 . 12	-	-	-	-
49.9	1.823	6	1 0 . 10	-	-	-	-
50.3	1.814	10	2 0 . 9	1.812	12	1.809	19
53.2	1.718	3	2 0 . 10	-	-	-	-
53.8	1.701	8	3 0 . 0	1.697	10	-	-
54.4	1.684	5	3 0 . 2	-	-	-	-
55.0	1.668	53	2 1 . 7	1.668	55	1.665	37
55.4	1.658	8	0 0 . 14	-	-	-	-
56.3	1.633	30	3 0 . 4	-	-	-	-
56.5	1.626	58	2 0 . 11	1.630	78	1.627	65
56.8	1.618	10	1 1 . 12	-	-	-	-
57.3	1.606	7	2 1 . 8	-	-	-	-
58.4	1.578	3	1 0 . 14	-	-	-	-
59.8	1.546	2	2 1 . 9	-	-	-	-
59.9	1.541	3	2 0 . 12	-	-	-	-
62.5	1.484	2	2 1 . 10	-	-	-	-
62.7	1.481	6	1 0 . 15	-	-	-	-
63.0	1.474	63	2 2 . 0	1.474	54	1.474	79
63.5	1.463	5	2 0 . 13	-	-	-	-
64.1	1.451	<1	0 0 . 16	-	-	-	-
65.5	1.424	3	2 1 . 11	-	-	-	-
67.3	1.390	13	2 0 . 14	1.388	14	1.392	<1
68.0	1.377	4	2 2 . 6	-	-	-	-
71.7	1.314	9	2 2 . 8	-	-	-	-
72.0	1.310	4	2 1 . 13	1.310	7	-	-
72.5	1.302	15	3 1 . 7	1.304	27	1.304	26
74.1	1.278	3	3 0 . 12	-	-	-	-
75.4	1.259	6	4 0 . 3	-	-	-	-

Table 9 : 2 θ 's, interplaner spacings and intensities of various peaks observed in XRD of nickel substituted barium ferrite of composition BaFe_{12-x}Ni_xO_{19-x/2}

x= 0 Standard data				x= 0 Observed		x=0.6 Observed	
2 θ°	d(Å)	Relative intensity	h k l	d(Å)	Relative intensity	d (Å)	Relative Intensity
22.9	3.868	18	0 0 . 6	3.847	8	3.864	7
30.2	2.948	55	1 1 . 0	2.938	40	2.938	70
30.8	2.901	32	0 0 . 8	2.901	36	2.901	44
31.3	2.859	9	1 1 . 2	-	-	-	-
32.1	2.782	100	1 0 . 7	2.786	100	2.786	96
34.1	2.628	98	1 1 . 4	2.627	97	2.627	100
35.1	2.553	11	2 0 . 0	-	-	-	-
35.6	2.522	10	1 0 . 8	-	-	2.540	34
37.0	2.425	60	2 0 . 3	2.428	50	2.421	43
38.7	2.322	<1	0 0 . 10	-	-	-	-
39.1	2.303	4	1 0 . 9	-	-	-	-
40.3	2.237	29	2 0 . 5	2.231	35	2.225	29
42.4	2.131	18	2 0 . 6	2.130	23	2.125	20
42.8	2.113	3	1 0 . 10	-	-	-	-
46.4	1.949	9	1 0 . 11	1.947	9	-	-
46.9	1.934	<1	0 0 . 12	-	-	-	-
49.9	1.823	6	1 0 . 10	-	-	-	-
50.3	1.814	10	2 0 . 9	1.812	12	1.812	10
53.2	1.718	3	2 0 . 10	-	-	-	-
53.8	1.701	8	3 0 . 0	1.697	10	1.669	5
54.4	1.684	5	3 0 . 2	-	-	-	-
55.0	1.668	53	2 1 . 7	1.668	55	1.665	40
55.4	1.658	8	0 0 . 14	-	-	-	-
56.3	1.633	30	3 0 . 4	-	-	-	-
56.5	1.626	58	2 0 . 11	1.630	78	1.625	74
56.8	1.618	10	1 1 . 12	-	-	-	-
57.3	1.606	7	2 1 . 8	-	-	1.612	47
58.4	1.578	3	1 0 . 14	-	-	-	-
59.8	1.546	2	2 1 . 9	-	-	-	-
59.9	1.541	3	2 0 . 12	-	-	-	-
62.5	1.484	2	2 1 . 10	-	-	-	-
62.7	1.481	6	1 0 . 15	-	-	-	-
63.0	1.474	63	2 2 . 0	1.474	54	1.472	61
63.5	1.463	5	2 0 . 13	-	-	-	-
64.1	1.451	<1	0 0 . 16	-	-	-	-
65.5	1.424	3	2 1 . 11	-	-	1.424	10
67.3	1.390	13	2 0 . 14	1.388	14	1.388	20
68.0	1.377	4	2 2 . 6	-	-	-	-
71.7	1.314	9	2 2 . 8	-	-	-	-
72.0	1.310	4	2 1 . 13	1.310	7	1.310	10
72.5	1.302	15	3 1 . 7	1.304	27	1.300	16
74.1	1.278	3	3 0 . 12	-	-	-	-
75.4	1.259	6	4 0 . 3	-	-	-	-

Table 10 : 2θ 's, interplaner spacings and intensities of various peaks observed in XRD of nickel substituted barium ferrite of composition $\text{BaFe}_{12-x}\text{Ni}_x\text{O}_{19-x/2}$

x = 0 Standard data				x=0 Observed		x=0.8 Observed	
$2\theta^\circ$	d(Å)	Relative intensity	h k .l	d(Å)	Relative intensity	d (Å)	Relative Intensity
22.9	3.868	18	0 0 . 6	3.847	8	3.847	15
30.2	2.948	55	1 1 . 0	2.938	40	-	-
30.8	2.901	32	0 0 . 8	2.901	36	2.919	96
31.3	2.859	9	1 1 . 2	-	-	-	-
32.1	2.782	100	1 0 . 7	2.786	100	2.761	100
34.1	2.628	98	1 1 . 4	2.627	97	2.612	99
35.1	2.553	11	2 0 . 0	-	-	-	-
35.6	2.522	10	1 0 . 8	-	-	2.495	95
37.0	2.425	60	2 0 . 3	2.428	50	2.419	62
38.7	2.322	<1	0 0 . 10	-	-	-	-
39.1	2.303	4	1 0 . 9	-	-	-	-
40.3	2.237	29	2 0 . 5	2.231	35	2.225	11
42.4	2.131	18	2 0 . 6	2.130	23	2.120	26
42.8	2.113	3	1 0 . 10	-	-	-	-
46.4	1.949	9	1 0 . 11	1.947	9	-	-
46.9	1.934	<1	0 0 . 12	-	-	-	-
49.9	1.823	6	1 0 . 10	-	-	-	-
50.3	1.814	10	2 0 . 9	1.812	12	1.809	14
53.2	1.718	3	2 0 . 10	-	-	1.717	<1
53.8	1.701	8	3 0 . 0	1.697	10	-	-
54.4	1.684	5	3 0 . 2	-	-	-	-
55.0	1.668	53	2 1 . 7	1.668	55	1.663	88
55.4	1.658	8	0 0 . 14	-	-	-	-
56.3	1.633	30	3 0 . 4	-	-	-	-
56.5	1.626	58	2 0 . 11	1.630	78	-	-
56.8	1.618	10	1 1 . 12	-	-	-	-
57.3	1.606	7	2 1 . 8	-	-	-	-
58.4	1.578	3	1 0 . 14	-	-	-	-
59.8	1.546	2	2 1 . 9	-	-	-	-
59.9	1.541	3	2 0 . 12	-	-	-	-
62.5	1.484	2	2 1 . 10	-	-	-	-
62.7	1.481	6	1 0 . 15	-	-	-	-
63.0	1.474	63	2 2 . 0	1.474	54	1.466	95
63.5	1.463	5	2 0 . 13	-	-	-	-
64.1	1.451	<1	0 0 . 16	-	-	-	-
65.5	1.424	3	2 1 . 11	-	-	-	-
67.3	1.390	13	2 0 . 14	1.388	14	1.386	5
68.0	1.377	4	2 2 . 6	-	-	-	-
71.7	1.314	9	2 2 . 8	-	-	-	-
72.0	1.310	4	2 1 . 13	1.310	7	-	-
72.5	1.302	15	3 1 . 7	1.304	27	1.293	21
74.1	1.278	3	3 0 . 12	-	-	-	-
75.4	1.259	6	4 0 . 3	-	-	1.264	9

Table 11 : 2θ 's, interplaner spacings and intensities of various peaks observed in XRD of nickel substituted barium ferrite of composition $\text{BaFe}_{12-x}\text{Ni}_x\text{O}_{19-x/2}$

x=0 Standard data				x=0 Observed		x=1.0 Observed	
$2\theta^\circ$	d(Å)	Relative intensity	h k l	d(Å)	Relative intensity	d (Å)	Relative Intensity
22.9	3.868	18	0 0 6	3.847	8	3.864	13
30.2	2.948	55	1 1 0	2.938	40	2.938	73
30.8	2.901	32	0 0 8	2.901	36	2.901	65
31.3	2.859	9	1 1 2	-	-	-	-
32.1	2.782	100	1 0 7	2.786	100	2.778	100
34.1	2.628	98	1 1 4	2.627	97	2.627	93
35.1	2.553	11	2 0 0	-	-	-	-
35.6	2.522	10	1 0 8	-	-	2.513	62
37.0	2.425	60	2 0 3	2.428	50	2.415	50
38.7	2.322	<1	0 0 10	-	-	-	-
39.1	2.303	4	1 0 9	-	-	-	-
40.3	2.237	29	2 0 5	2.231	35	2.231	21
42.4	2.131	18	2 0 6	2.130	23	2.120	21
42.8	2.113	3	1 0 10	-	-	-	-
46.4	1.949	9	1 0 11	1.947	9	-	-
46.9	1.934	<1	0 0 12	-	-	-	-
49.9	1.823	6	1 0 10	-	-	-	-
50.3	1.814	10	2 0 9	1.812	12	1.809	8
53.2	1.718	3	2 0 10	-	-	-	-
53.8	1.701	8	3 0 0	1.697	10	-	-
54.4	1.684	5	3 0 2	-	-	-	-
55.0	1.668	53	2 1 7	1.668	55	1.663	41
55.4	1.658	8	0 0 14	-	-	-	-
56.3	1.633	30	3 0 4	-	-	-	-
56.5	1.626	58	2 0 11	1.630	78	1.625	63
56.8	1.618	10	1 1 12	-	-	-	-
57.3	1.606	7	2 1 8	-	-	-	-
58.4	1.578	3	1 0 14	-	-	-	-
59.8	1.546	2	2 1 9	-	-	-	-
59.9	1.541	3	2 0 12	-	-	-	-
62.5	1.484	2	2 1 10	-	-	-	-
62.7	1.481	6	1 0 15	-	-	-	-
63.0	1.474	63	2 2 0	1.474	54	1.472	61
63.5	1.463	5	2 0 13	-	-	-	-
64.1	1.451	<1	0 0 16	-	-	-	-
65.5	1.424	3	2 1 11	-	-	-	-
67.3	1.390	13	2 0 14	1.388	14	-	-
68.0	1.377	4	2 2 6	-	-	-	-
71.7	1.314	9	2 2 8	-	-	-	-
72.0	1.310	4	2 1 13	1.310	7	-	-
72.5	1.302	15	3 1 7	1.304	27	1.298	12
74.1	1.278	3	3 0 12	-	-	-	-
75.4	1.259	6	4 0 3	-	-	-	-

Table 12: 2 θ 's, interplaner spacings and intensities of various peaks observed in XRD of nickel and titanium substituted barium ferrite BaFe_{12-2x}Ni_xTi_xO₁₉

x= 0 Standard data				x=0 Observed		x=1.2 Observed	
2 θ°	d(Å)	Relative intensity	h k .l	d(Å)	Relative intensity	d (Å)	Relative Intensity
22.9	3.868	18	0 0 . 6	3.847	8	-	-
30.2	2.948	55	1 1 . 0	2.938	40	2.938	84
30.8	2.901	32	0 0 . 8	2.901	36	-	-
31.3	2.859	9	1 1 . 2	-	-	-	-
32.1	2.782	100	1 0 . 7	2.786	100	2.786	96
34.1	2.628	98	1 1 . 4	2.627	97	2.627	100
35.1	2.553	11	2 0 . 0	-	-	-	-
35.6	2.522	10	1 0 . 8	-	-	2.526	78
37.0	2.425	60	2 0 . 3	2.428	50	2.421	22
38.7	2.322	<1	0 0 . 10	-	-	-	-
39.1	2.303	4	1 0 . 9	-	-	-	-
40.3	2.237	29	2 0 . 5	2.231	35	2.236	22
42.4	2.131	18	2 0 . 6	2.130	23	2.125	19
42.8	2.113	3	1 0 . 10	-	-	2.079	13
46.4	1.949	9	1 0 . 11	1.947	9	-	-
46.9	1.934	<1	0 0 . 12	-	-	-	-
49.9	1.823	6	1 0 . 10	-	-	-	-
50.3	1.814	10	2 0 . 9	1.812	12	-	-
53.2	1.718	3	2 0 . 10	-	-	-	-
53.8	1.701	8	3 0 . 0	1.697	10	1.721	17
54.4	1.684	5	3 0 . 2	-	-	-	-
55.0	1.668	53	2 1 . 7	1.668	55	1.665	44
55.4	1.658	8	0 0 . 14	-	-	-	-
56.3	1.633	30	3 0 . 4	-	-	-	-
56.5	1.626	58	2 0 . 11	1.630	78	-	-
56.8	1.618	10	1 1 . 12	-	-	1.627	76
57.3	1.606	7	2 1 . 8	-	-	1.607	52
58.4	1.578	3	1 0 . 14	-	-	-	-
59.8	1.546	2	2 1 . 9	-	-	-	-
59.9	1.541	3	2 0 . 12	-	-	-	-
62.5	1.484	2	2 1 . 10	-	-	-	-
62.7	1.481	6	1 0 . 15	-	-	-	-
63.0	1.474	63	2 2 . 0	1.474	54	1.474	81
63.5	1.463	5	2 0 . 13	-	-	-	-
64.1	1.451	<1	0 0 . 16	-	-	-	-
65.5	1.424	3	2 1 . 11	-	-	-	-
67.3	1.390	13	2 0 . 14	1.388	14	1.392	14
68.0	1.377	4	2 2 . 6	-	-	-	-
71.7	1.314	9	2 2 . 8	-	-	-	-
72.0	1.310	4	2 1 . 13	1.310	7	-	-
72.5	1.302	15	3 1 . 7	1.304	27	1.303	16
74.1	1.278	3	3 0 . 12	-	-	-	-
75.4	1.259	6	4 0 . 3	-	-	-	-

Table 13 : 2θ 's, interplaner spacings and intensities of various peaks observed in XRD of nickel substituted barium ferrite of composition $\text{BaFe}_{12-x}\text{Ni}_x\text{O}_{19-x/2}$

x= 0 Standard data				x=0 Observed		x=1.4 Observed	
$2\theta^\circ$	d(Å)	Relative intensity	h k .l	d(Å)	Relative intensity	d (Å)	Relative Intensity
22.9	3.868	18	0 0 . 6	3.847	8	-	-
30.2	2.948	55	1 1 . 0	2.938	40	2.928	89
30.8	2.901	32	0 0 . 8	2.901	36	-	-
31.3	2.859	9	1 1 . 2	-	-	-	-
32.1	2.782	100	1 0 . 7	2.786	100	2.786	90
34.1	2.628	98	1 1 . 4	2.627	97	2.620	84
35.1	2.553	11	2 0 . 0	-	-	-	-
35.6	2.522	10	1 0 . 8	-	-	2.513	100
37.0	2.425	60	2 0 . 3	2.428	50	2.428	54
38.7	2.322	<1	0 0 . 10	-	-	-	-
39.1	2.303	4	1 0 . 9	-	-	-	-
40.3	2.237	29	2 0 . 5	2.231	35	2.225	19
42.4	2.131	18	2 0 . 6	2.130	23	2.123	19
42.8	2.113	3	1 0 . 10	-	-	2.088	17
46.4	1.949	9	1 0 . 11	1.947	9	-	-
46.9	1.934	<1	0 0 . 12	-	-	-	-
49.9	1.823	6	1 0 . 10	-	-	-	-
50.3	1.814	10	2 0 . 9	1.812	12	-	-
53.2	1.718	3	2 0 . 10	-	-	-	-
53.8	1.701	8	3 0 . 0	1.697	10	-	-
54.4	1.684	5	3 0 . 2	-	-	1.691	20
55.0	1.668	53	2 1 . 7	1.668	55	1.663	47
55.4	1.658	8	0 0 . 14	-	-	-	-
56.3	1.633	30	3 0 . 4	-	-	-	-
56.5	1.626	58	2 0 . 11	1.630	78	-	-
56.8	1.618	10	1 1 . 12	-	-	1.627	60
57.3	1.606	7	2 1 . 8	-	-	1.604	50
58.4	1.578	3	1 0 . 14	-	-	-	-
59.8	1.546	2	2 1 . 9	-	-	-	-
59.9	1.541	3	2 0 . 12	-	-	1.538	8
62.5	1.484	2	2 1 . 10	-	-	-	-
62.7	1.481	6	1 0 . 15	-	-	-	-
63.0	1.474	63	2 2 . 0	1.474	54	1.472	76
63.5	1.463	5	2 0 . 13	-	-	1.466	69
64.1	1.451	<1	0 0 . 16	-	-	-	-
65.5	1.424	3	2 1 . 11	-	-	-	-
67.3	1.390	13	2 0 . 14	1.388	14	-	-
68.0	1.377	4	2 2 . 6	-	-	-	-
71.7	1.314	9	2 2 . 8	-	-	-	-
72.0	1.310	4	2 1 . 13	1.310	7	-	-
72.5	1.302	15	3 1 . 7	1.304	27	1.300	14
74.1	1.278	3	3 0 . 12	-	-	-	-
75.4	1.259	6	4 0 . 3	-	-	-	-

Table 14 : 2θ 's, interplaner spacings and intensities of various peaks observed in XRD of nickel substituted barium ferrite of composition $\text{BaFe}_{12-x}\text{Ni}_x\text{O}_{19-x/2}$

x= 0 Standard data				x=0 Observed		x=1.6 Observed	
$2\theta^\circ$	d(Å)	Relative intensity	h k .l	d(Å)	Relative intensity	d (Å)	Relative Intensity
22.9	3.868	18	0 0 . 6	3.847	8	-	-
30.2	2.948	55	1 1 . 0	2.938	40	2.947	82
30.8	2.901	32	0 0 . 8	2.901	36	2.882	59
31.3	2.859	9	1 1 . 2	-	-	-	-
32.1	2.782	100	1 0 . 7	2.786	100	2.786	78
34.1	2.628	98	1 1 . 4	2.627	97	2.627	52
35.1	2.553	11	2 0 . 0	-	-	-	-
35.6	2.522	10	1 0 . 8	-	-	2.519	100
37.0	2.425	60	2 0 . 3	2.428	50	2.428	51
38.7	2.322	<1	0 0 . 10	-	-	-	-
39.1	2.303	4	1 0 . 9	-	-	-	-
40.3	2.237	29	2 0 . 5	2.231	35	2.241	13
42.4	2.131	18	2 0 . 6	2.130	23	-	-
42.8	2.113	3	1 0 . 10	-	-	-	-
46.4	1.949	9	1 0 . 11	1.947	9	-	-
46.9	1.934	<1	0 0 . 12	-	-	-	-
49.9	1.823	6	1 0 . 10	-	-	-	-
50.3	1.814	10	2 0 . 9	1.812	12	-	-
53.2	1.718	3	2 0 . 10	-	-	-	-
53.8	1.701	8	3 0 . 0	1.697	10	1.670	20
54.4	1.684	5	3 0 . 2	-	-	-	-
55.0	1.668	53	2 1 . 7	1.668	55	1.665	43
55.4	1.658	8	0 0 . 14	-	-	-	-
56.3	1.633	30	3 0 . 4	-	-	-	-
56.5	1.626	58	2 0 . 11	1.630	78	-	-
56.8	1.618	10	1 1 . 12	-	-	1.627	50
57.3	1.606	7	2 1 . 8	-	-	1.607	47
58.4	1.578	3	1 0 . 14	-	-	-	-
59.8	1.546	2	2 1 . 9	-	-	-	-
59.9	1.541	3	2 0 . 12	-	-	-	-
62.5	1.484	2	2 1 . 10	-	-	-	-
62.7	1.481	6	1 0 . 15	-	-	-	-
63.0	1.474	63	2 2 . 0	1.474	54	1.425	66
63.5	1.463	5	2 0 . 13	-	-	-	-
64.1	1.451	<1	0 0 . 16	-	-	-	-
65.5	1.424	3	2 1 . 11	-	-	-	-
67.3	1.390	13	2 0 . 14	1.388	14	1.466	7
68.0	1.377	4	2 2 . 6	-	-	-	-
71.7	1.314	9	2 2 . 8	-	-	-	-
72.0	1.310	4	2 1 . 13	1.310	7	-	-
72.5	1.302	15	3 1 . 7	1.304	27	1.301	14
74.1	1.278	3	3 0 . 12	-	-	-	-
75.4	1.259	6	4 0 . 3	-	-	-	-

Table 15 : 2θ 's, interplaner spacings and intensities of various peaks observed in XRD of standard NiFe_2O_4 and standard $\text{BaFe}_{12}\text{O}_{19}$.

NiFe_2O_4 Standard data				$\text{BaFe}_{12}\text{O}_{19}$ Standard data		
$2\theta^\circ$	$d(\text{\AA})$	hkl	Relative Intensity	$d(\text{\AA})$	hk.l	Relative Intensity
17.8	-	-	-	4.99	10.1	7
18.4	4.813	111	11	-	-	-
19.0	-	-	-	4.673	10.2	14
22.9	-	-	-	3.868	00.6	18
30.3	2.948	220	33	2.948	11.0	55
30.8	-	-	-	2.901	00.8	32
31.3	-	-	-	2.859	11.2	9
32.1	-	-	-	2.782	10.7	100
34.1	-	-	-	2.628	11.4	98
35.1	-	-	-	2.553	20.0	11
35.6	-	-	-	2.522	10.8	10
35.7	2.514	311	100	-	-	-
37.1	-	-	-	2.425	20.3	60
37.2	2.407	222	7	-	-	-
40.3	-	-	-	2.237	20.5	29
42.4	-	-	-	2.130	20.6	18
42.7	-	-	-	2.113	10.10	3
43.4	2.085	400	22	-	-	-
50.3	-	-	-	1.814	20.9	10
53.3	-	-	-	1.718	20.10	9
53.8	1.702	422	9	1.701	30.0	8
55.0	-	-	-	1.668	21.7	53
56.3	-	-	-	1.633	30.4	30
56.9	-	-	-	1.626	20.11	58
56.5	-	-	-	1.618	11.12	10
57.4	1.605	511	28	-	-	-
63.0	1.474	440	34	1.474	22.0	63
67.3	-	-	-	1.390	20.14	13

This suggests that the area of the hysteresis loop decreases too with increase in nickel content. The magnetization vs. temperature (T) curves at a fixed magnetic field of 11kOe for samples of $\text{BaFe}_{12}\text{O}_{19}$ and others having nickel content $x = 0.6, 1.2$ and 1.4 are shown in Figs. 11 and 12. Clearly, the magnetization decreases continuously with increase of temperature up to a point beyond which the change is somewhat abrupt, indi-

cative of ferromagnetic to paramagnetic transition. Curie temperature (T_c) was determined as usual by the intersection of tangent, drawn at the point of highest slope in the M-H curve, with abscissa. The values obtained for (T_c) are listed in Table 16 and shown on M_s vs. T plots in Figs. 11 and 12. With increasing nickel content (x), Curie temperature is found to increase in $BaFe_{12-x}Ni_xO_{19-x/2}$ compounds, the values being 458°C and 474°C for $x=0$ and 1.4, respectively.

Table16 : Saturation magnetization and coercivity of different nickel containing barium ferrite $BaFe_{12-x}Ni_xO_{19-x/2}$

Amount of nickel Substitution (x)	Saturation Magnetization M_s (emu/g)	Coercivity H_c (Oe)	Curie Temperature T_c ($^\circ\text{C}$)
0	59.3 ± 0.1	4300 ± 0001	458
0.2	55.8 ± 0.1	3403 ± 0001	---
0.4	----	---	---
0.6	54.9 ± 0.1	2911 ± 0001	463
0.8	----	---	---
1.0	50.1 ± 0.1	2761 ± 0001	466
1.2	48.8 ± 0.1	2308 ± 0001	---
1.4	48.1 ± 0.1	2074 ± 0001	474
1.6	43.4 ± 0.1	1379 ± 0001	---

3.1.3 Mossbauer spectroscopic analysis

The Mossbauer spectra of $BaFe_{12-x}Ni_xO_{19-x/2}$ with $0 \leq x \leq 1.6$ at room temperature are shown in Figs. 13-15. These are fitted with various sextet sub-patterns corresponding to five different sites $4f_{iv}$, $4f_{vi}$, 2a, 2b and 12k of pure barium ferrite. The values corresponding to hyperfine field and spectral area for of $BaFe_{12-x}Ni_xO_{19-x/2}$ with $0 \leq x \leq 1.6$ are given in

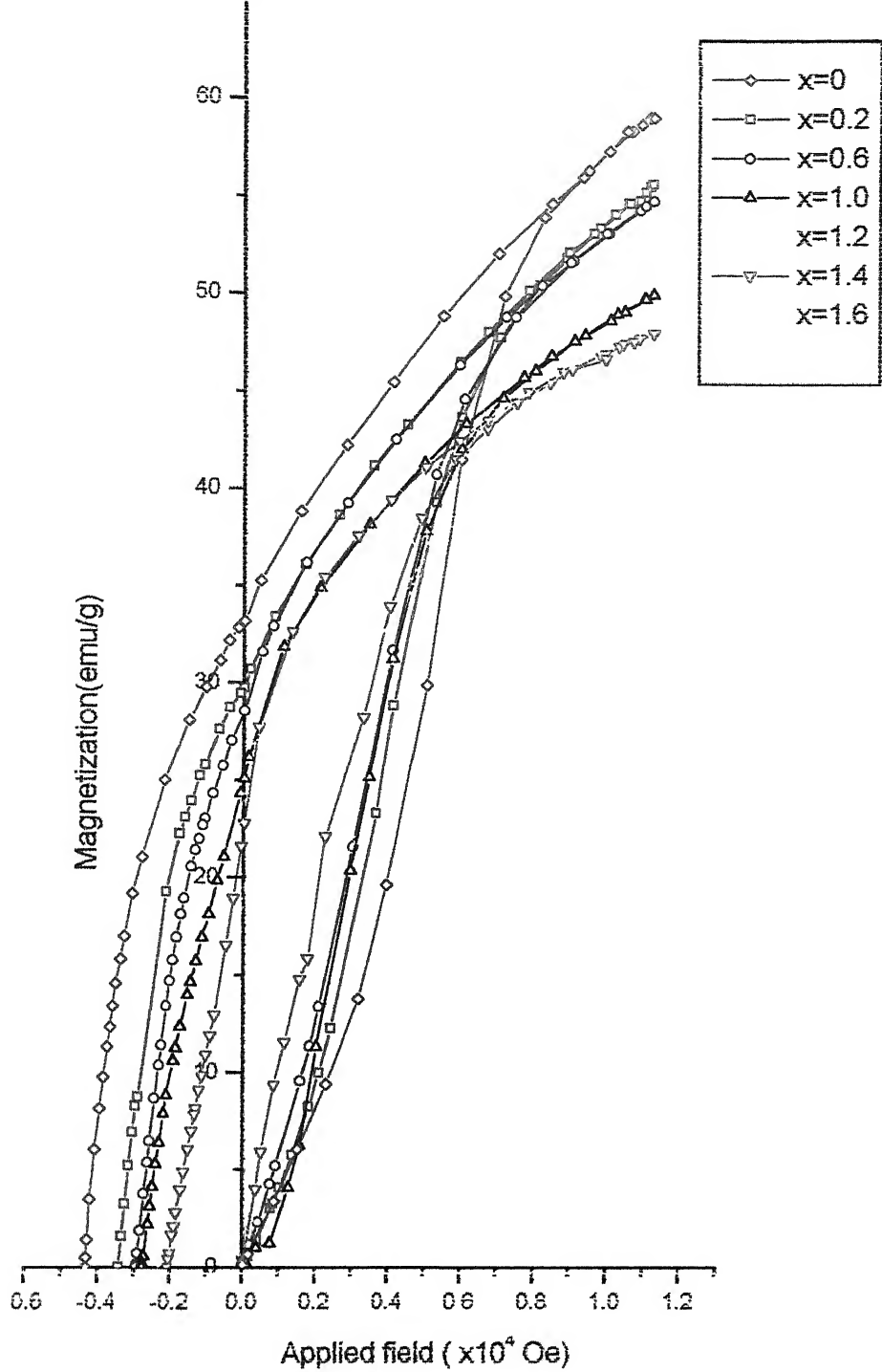


Fig 8 : Magnetization vs applied field curve for
nickel substituted barium ferrite $\text{BaFe}_{12-x}\text{Ni}_x\text{O}_{19}$

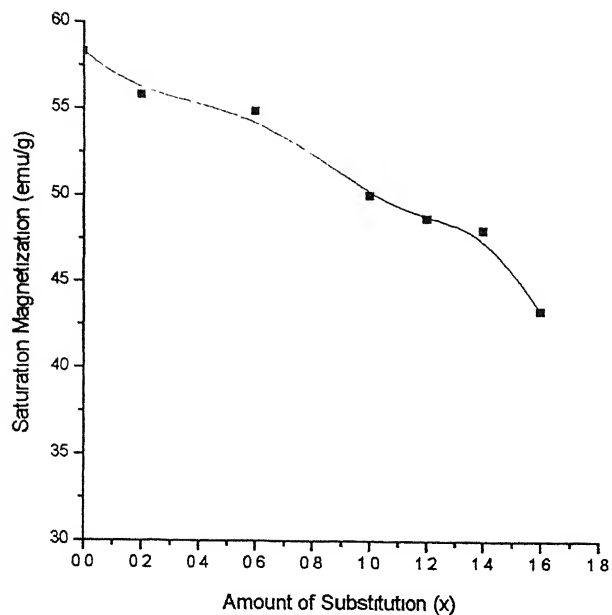


Fig. 9: Saturation magnetization for $\text{BaFe}_{12-x}\text{Ni}_x\text{O}_{19-x/2}$ vs. amount of substitution (x)

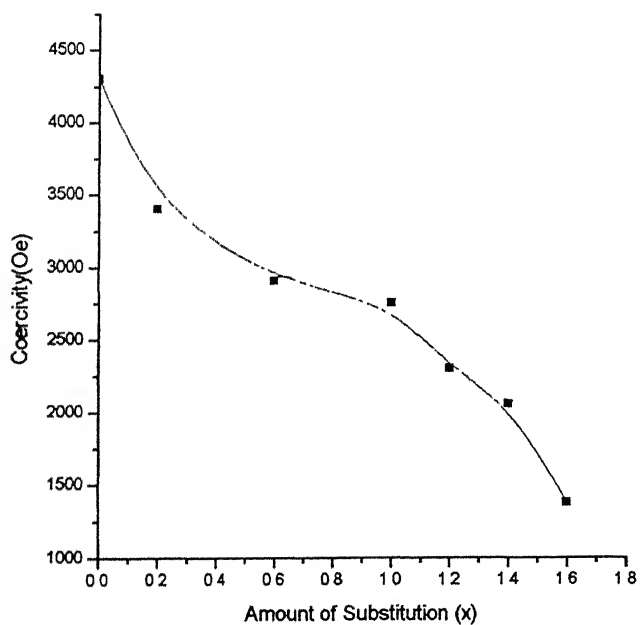


Fig. 10: Coercivity of $\text{BaFe}_{12-x}\text{Ni}_x\text{O}_{19-x/2}$ vs. amount of substitution (x)

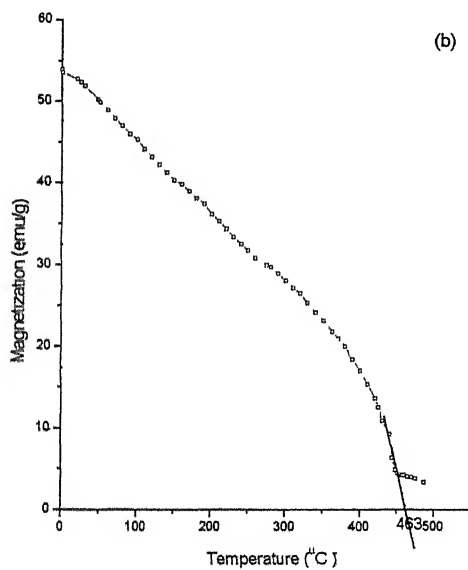
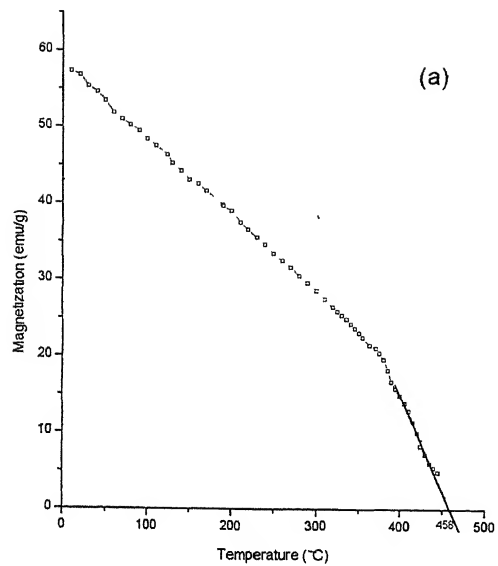


Fig. 11: Variation of magnetization with temperature of barium ferrite of composition $\text{BaFe}_{12-x}\text{Ni}_x\text{O}_{19-x/2}$ with (a) $x=0$ and (b) $x=0.6$

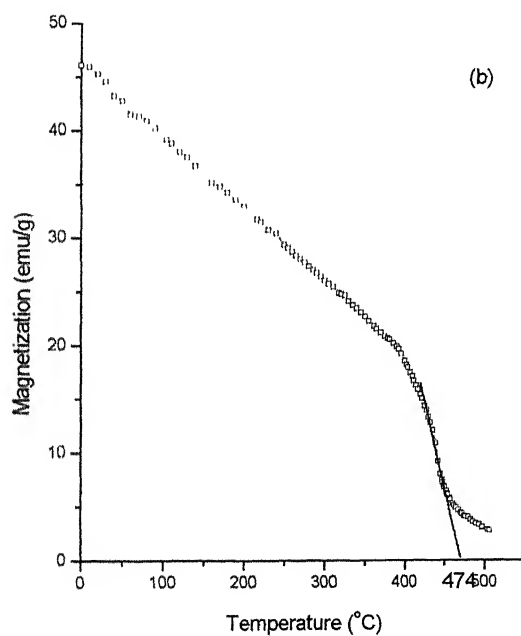
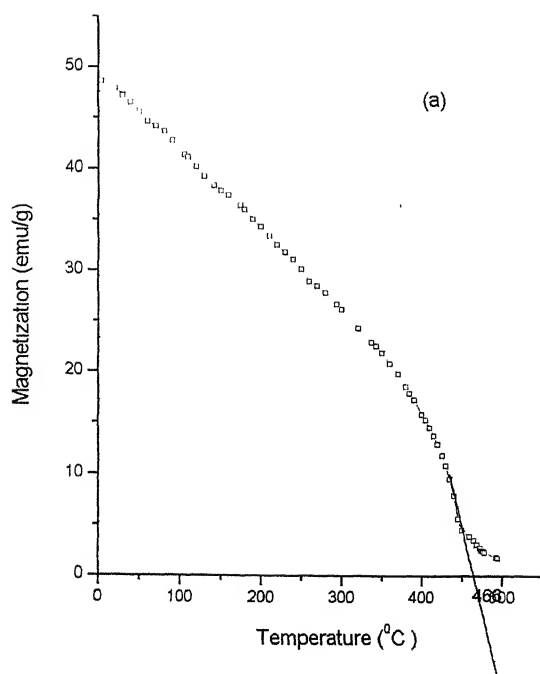


Fig 12: Variation of Magnetization with barium ferrite of composition $\text{BaFe}_{12-x}\text{Ni}_x\text{O}_{19-x/2}$ with (a) $x=1.2$ and (b) $x=1.4$

Table 17. The variation of hyperfine fields and relative spectral areas are shown schematically in Figs 16 and 17, respectively. The area under the sextet corresponds to the number of iron ions present at that particular site. The small 2b area suggests that the recoil-free fraction be reduced for this site due to unusually large vibration amplitude [28]. The relative spectral areas of sextets corresponding to crystallographic sites 12k and 2b decrease while that of $4f_{iv}$, $4f_{vi}$, and 2a sites vary randomly. These reflect that nickel is occupying 12k and 2b sites preferentially. The hyperfine fields for all sites except 12k decrease or remain almost constant with increase of substitution level within experimental limits of ± 3 kOe. The hyperfine field for the 12k site is though varying randomly. The Fe^{3+} ions in the trigonal 2b and octahedral $4f_{vi}$ sites are known to be responsible for uniaxial anisotropy of barium ferrite [17]. This suggest that substitution of nickel at the 2b site is mainly responsible for decrease in coercivity.

Albanese [15] has shown that hyperfine magnetic field (H_{hf}) decreases rapidly with temperature in $BaFe_{12}O_{19}$ for 12k sites only. Since atomic magnetic moment also decreases with temperature and is known to be proportional to H_{hf} , it is believed that substitution of iron at 12k site by Ni^{2+} ions are mainly responsible for the observed temperature dependence of saturation magnetization. It essentially occurs due to strong interaction prevailing between 12k and 2b (spin up) sites. Needless to say, there exists orientation interaction as well between 12k and $4f_{vi}$ (spin down) and $4f_{iv}$ (spin down) iron ions.

Saturation magnetization can be increased when non-magnetic or

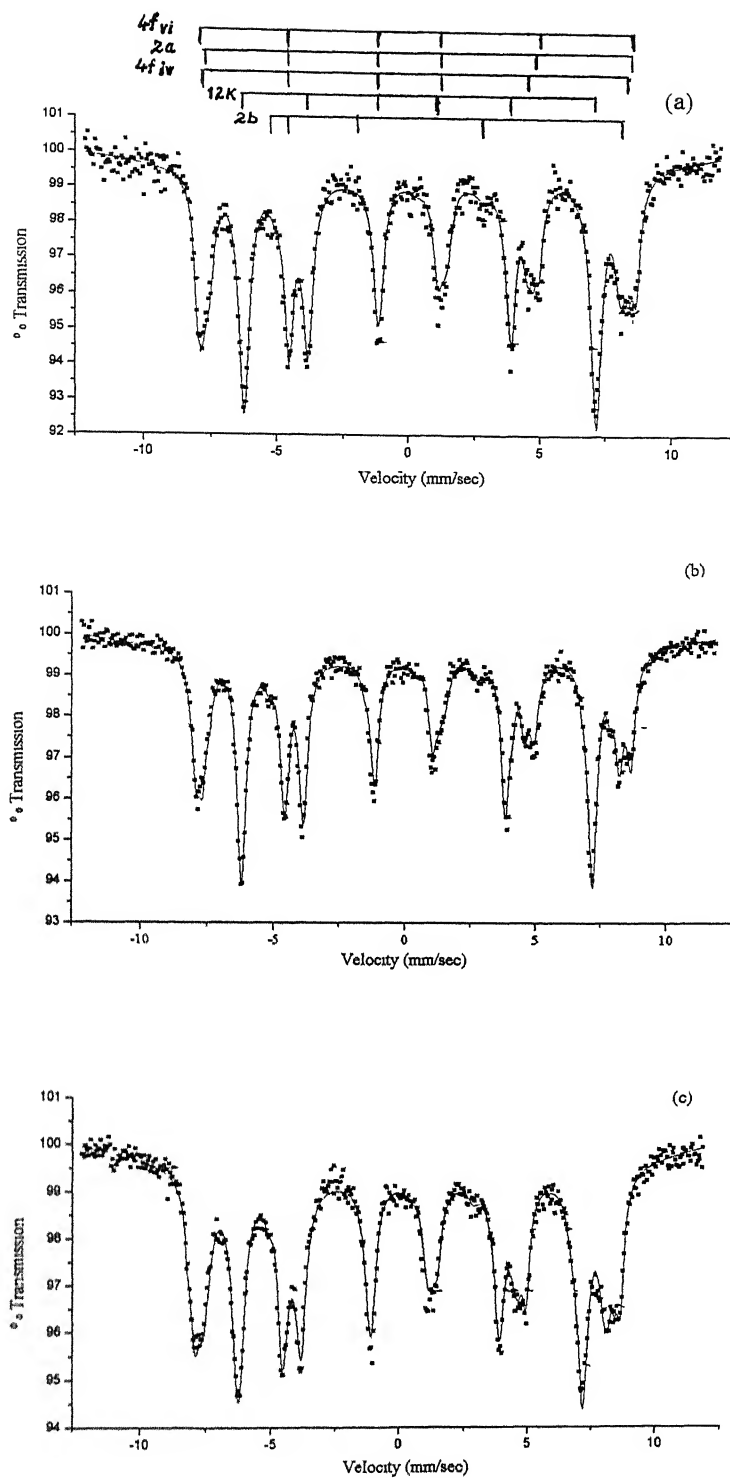


Fig 13· Mossbauer spectra of barium ferrite of composition $\text{BaFe}_{12-x}\text{Ni}_x\text{O}_{19-x/2}$ with (a) $x=0.0$ (b) $x=0.2$ (c) $x=0.4$

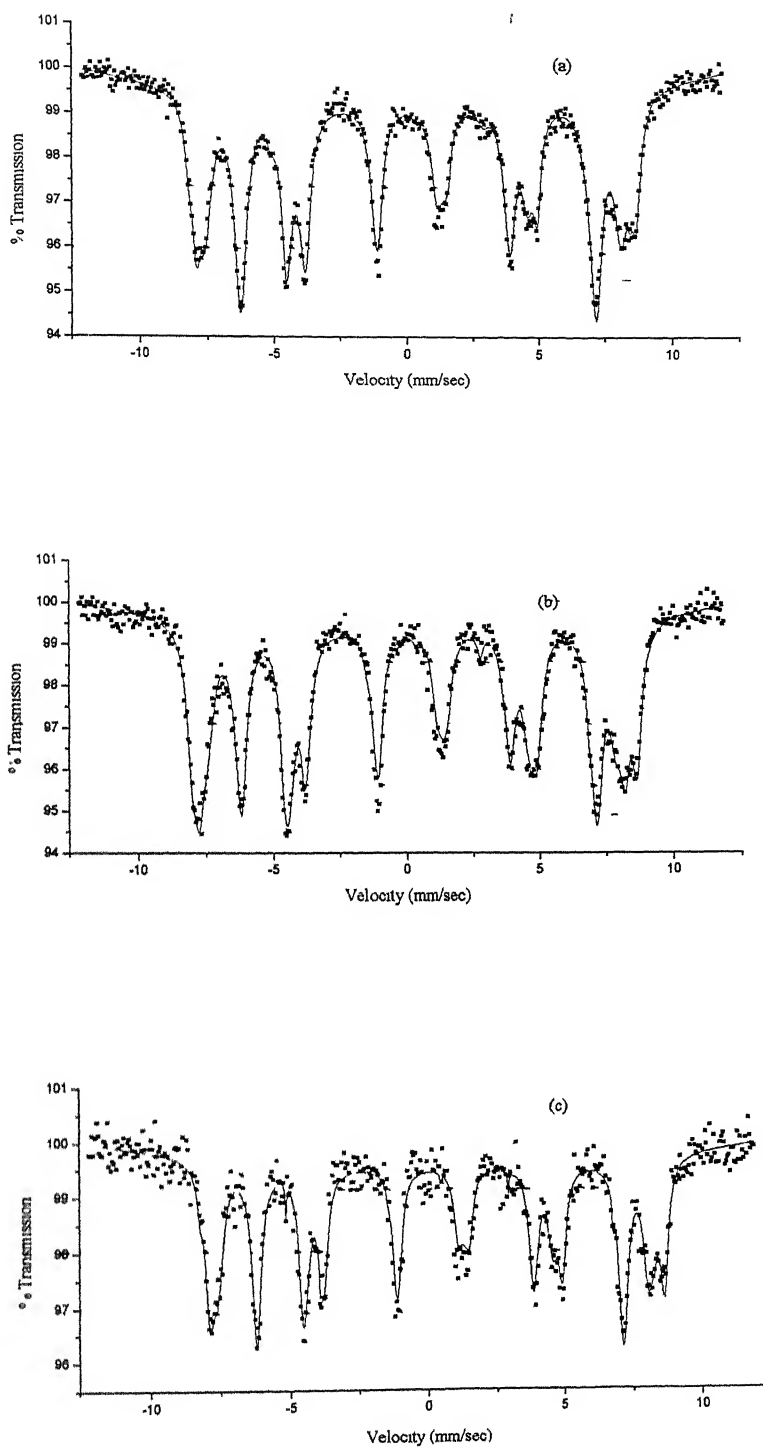


Fig 14: Mossbauer spectra of barium ferrite of composition $\text{BaFe}_{12-x}\text{Ni}_x\text{O}_{19-x/2}$ with (a) $x=0.6$ (b) $x=0.8$ (c) $x=1.0$

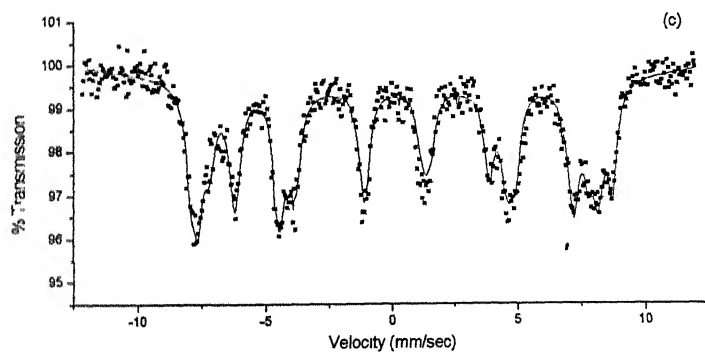
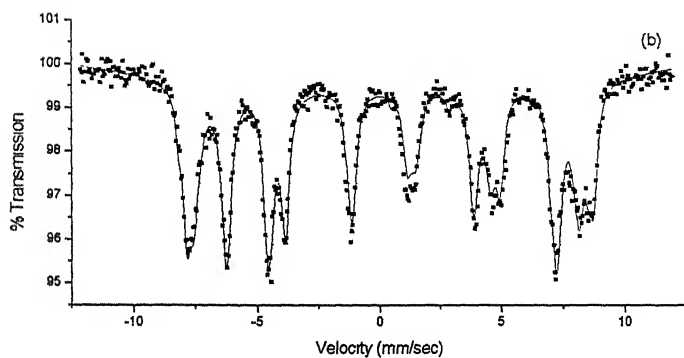
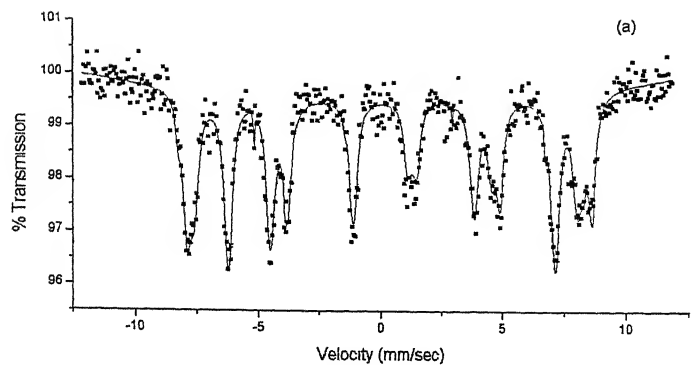


Fig 15: Mossbauer spectra of barium ferrite of composition $\text{BaFe}_{12-x}\text{Ni}_x\text{O}_{19-x/2}$ with (a) $x=1.2$ (b) $x=1.4$ (c) $x=1.6$

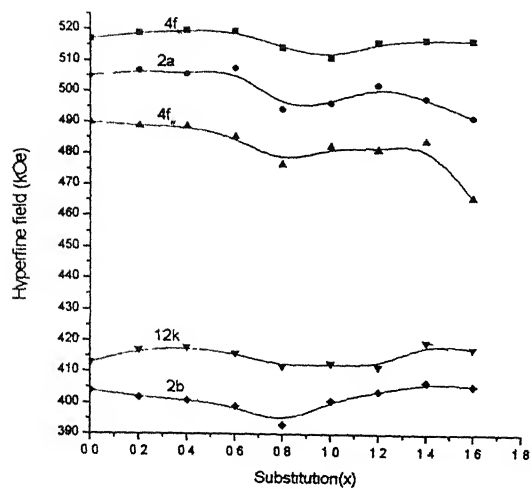


Fig. 16. Magnetic Hyperfine field for different sites in $\text{BaFe}_{12-x}\text{Ni}_x\text{O}_{19-x/2}$ at room temperature versus substitution

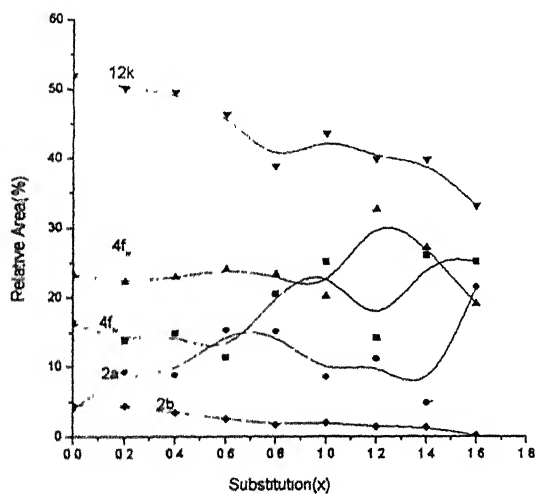


Fig. 17. Sextet area (normalized to 100%) of different sites in $\text{BaFe}_{12-x}\text{Ni}_x\text{O}_{19-x/2}$ at room temperature versus substitution

less magnetic ions than Fe^{3+} occupy spin down sites (i.e., f_{iv} , f_{vi}). On the other hand, saturation magnetization can be decreased by non-magnetic or less magnetic ions (with spin up) occupying 12k, 2a and 2b sites. The continuous decrease in saturation magnetization with increase of nickel content observed in $\text{BaFe}_{12-x}\text{Ni}_x\text{O}_{19-x/2}$ (Fig. 9) means that nickel ions are sitting in 12k, 2a and 2b sites. The Mossbauer spectra showing decrease in spectral areas of 12k and 2b sites further confirm this observation. Hence, the variation in saturation magnetization can be explained by occupancy of 12k and 2b sites by Ni^{2+} ions.

Table 17 : Relative spectral areas and hyperfine (Internal magnetic) fields of different crystallographic sites of barium ferrite of composition $\text{BaFe}_{12-x}\text{Ni}_x\text{O}_{19-x/2}$

Amount of substitution (x)	Site($4f_{vi}$)		Site(2a)		Site($4f_{iv}$)		Site(12k)		Site (2b)	
	Area (%)	Int. Mag Field (kOe)	Area (%)	Int. Mag Field (kOe)	Area (%)	Int. Mag Field (kOe)	Area (%)	Int. Mag Field (kOe)	Area (%)	Int. Mag Field (kOe)
0	16.39	517	4.00	505	23.32	490	51.88	413	4.58	404
0.2	13.81	519	9.30	507	22.30	489	50.15	417	4.43	402
0.4	14.98	520	8.91	506	23.02	489	49.60	418	3.56	401
0.6	11.38	520	15.44	508	24.15	486	46.41	416	2.59	399
0.8	20.58	515	15.23	495	23.41	477	38.97	412	1.80	393
1.0	25.28	512	8.63	497	20.22	483	43.78	413	2.07	401
1.2	14.26	517	11.28	503	32.89	482	40.10	412	1.44	404
1.4	26.18	518	4.95	499	27.27	485	40.14	420	1.43	407
1.6	25.40	518	21.73	493	19.27	467	33.43	418	0.156	406

3.2 Ni-Ti substituted ferrites

3.2.1 X-ray analysis

The XRD patterns of $\text{BaFe}_{12-2x}\text{Ni}_x\text{Ti}_x\text{O}_{19}$ with $0 \leq x \leq 1.0$ are shown

in Figs.18 and 19. The d-values and relative intensities of various diffraction peaks with their indices are given in Tables 18-22. The standard data of $\text{BaFe}_{12}\text{O}_{19}$ are also included for the sake of comparison. The indexing of XRD patterns suggest a hexagonal structure with unit cell with parameters as $a=5.867\pm0.001\text{\AA}$ and $c=23.310\pm0.001\text{\AA}$ for all the synthesized products. These data match reasonably well with known crystal data of pure barium ferrite having a magneto-plumbite structure with lattice parameters $a=5.895\text{ \AA}$, $c=23.215\text{ \AA}$, $Z=2$ and space group $p6_3/mmc$ [26]. The XRD patterns further depict that hexagonal magneto-plumbite structure is maintained for all the compositions.

3.2.2 Magnetic measurements

The magnetization versus applied field curves of nickel-titanium substituted barium ferrites of composition $\text{BaFe}_{12-2x}\text{Ni}_x\text{Ti}_x\text{O}_{19}$ with $x=0, 0.2, 0.4, 0.6, 0.8$ and 1.0 are shown in Fig. 20. The M_s vs. x plot (Fig. 21) depicts that the saturation magnetization lie in the range $52\text{--}59.3\text{ emu/g}$ for $0\leq x\leq 1.0$. Further, the coercivity H_c drops drastically from 4300 Oe to 1301 Oe as x increases from $x=0$ to 1.0 (Fig. 22). This decrease seems to be exponential in nature up to $x=0.8$ and follow the equation $H_c=H_{\infty}\exp(-\alpha x)$, where H_{∞} is the coercivity value for the case of $x=0$ and α is a constant ($=0.4$). The saturation magnetization, coercivity and Curie temperature of Ni-Ti substituted barium ferrites of composition $\text{BaFe}_{12-2x}\text{Ni}_x\text{Ti}_x\text{O}_{19}$ are given in Table 23. The magnetization vs. temperature curves for $x=0.2$ and 1.0 at the fixed magnetic field of 11kOe (Fig. 23) in conjunction with the case of pure barium ferrite (Fig. 11) indicate sharp decrease in magnetization progressively at low tempera-

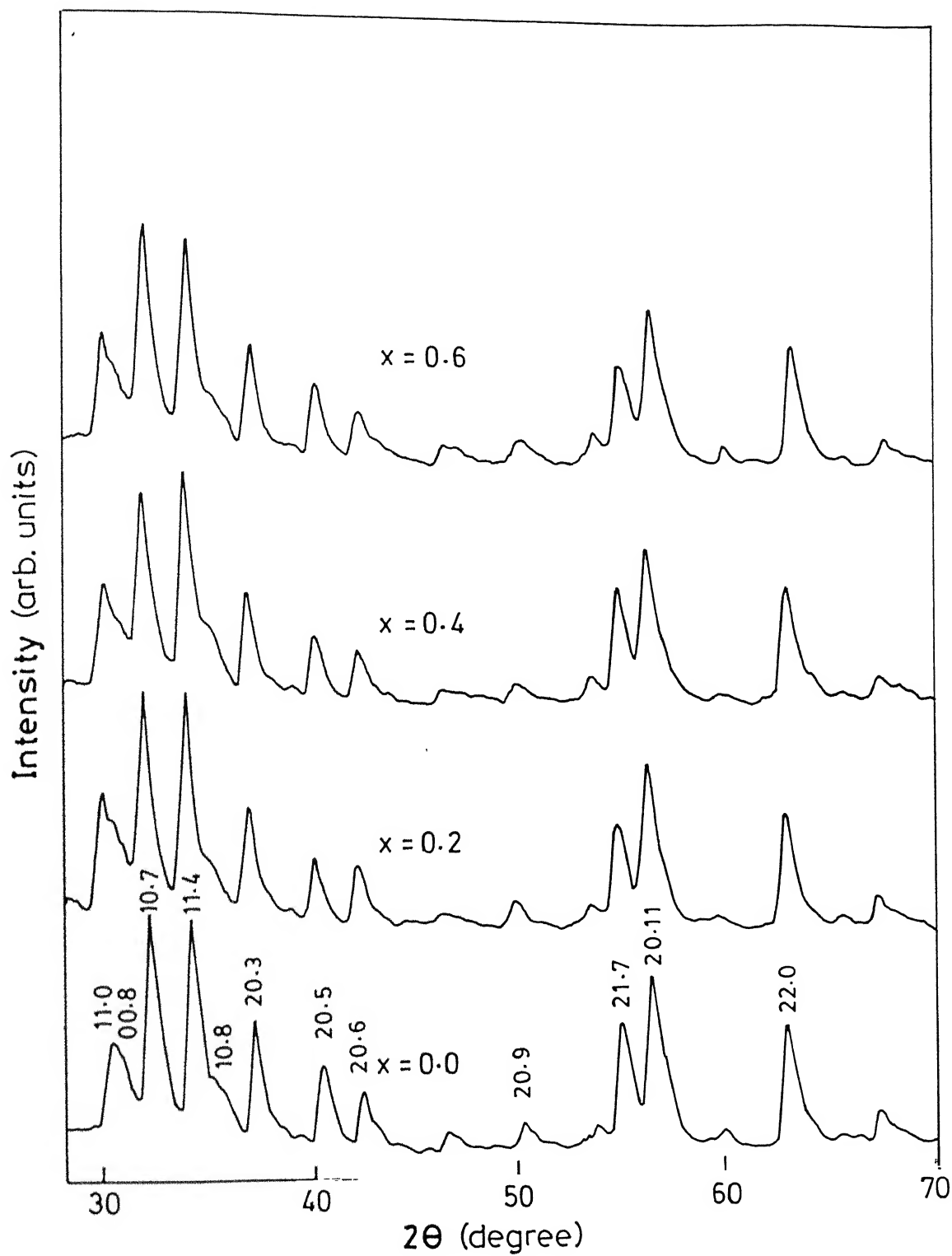


Fig . 18: XRD Pattern of barium hexa-ferrite of composition $\text{BaFe}_{12-2x}\text{Ni}_x\text{Ti}_x\text{O}_{19-x/2}$ with $x=0, 0.2, 0.4$ and 0.6 .

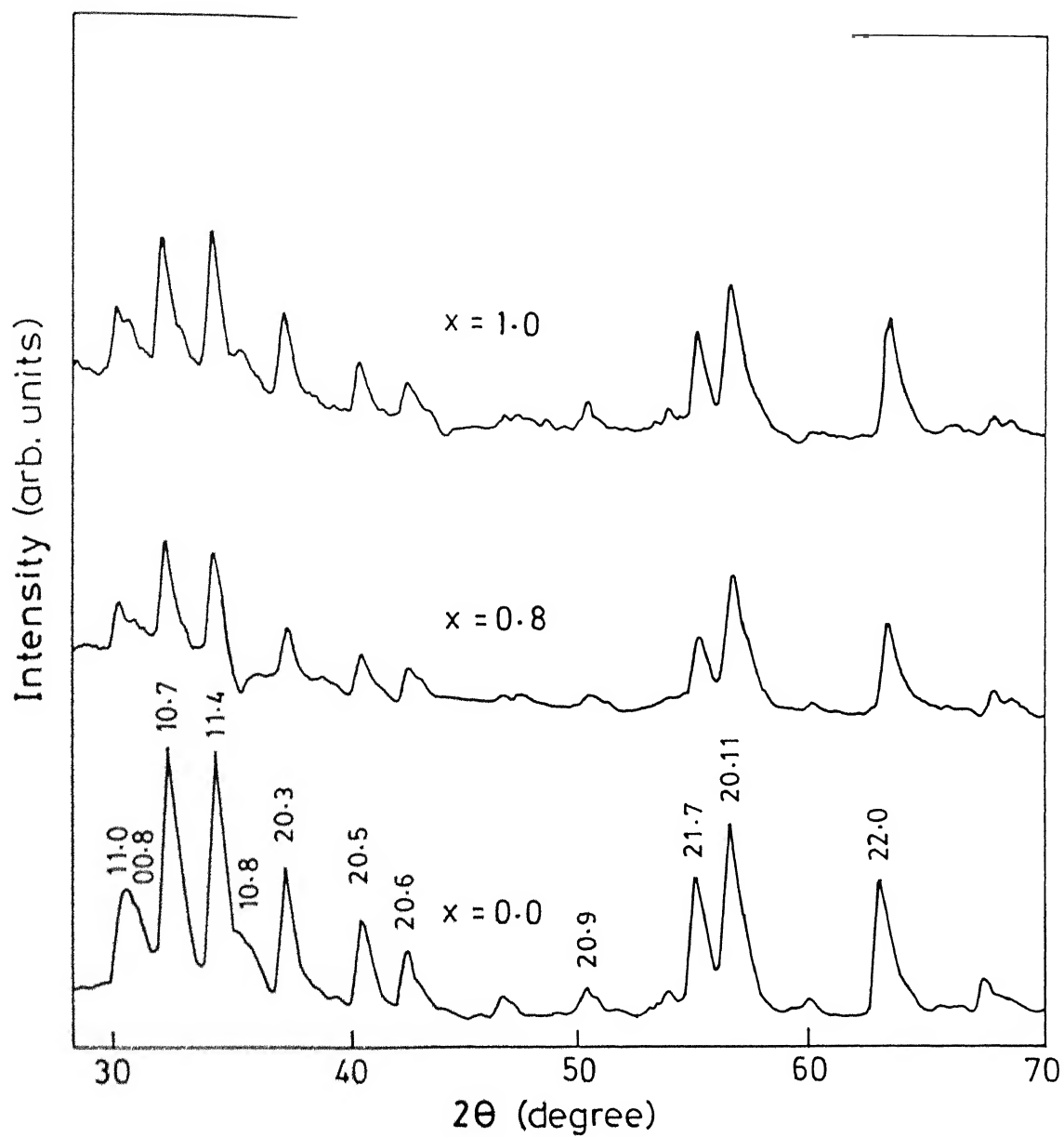


Fig . 19: XRD Pattern of barium hexa-ferrite of composition $\text{BaFe}_{12-2x}\text{Ni}_x\text{Ti}_x\text{O}_{19-x/2}$ with $x=0, 0.8, \text{ and } 1.0$.

Table 18 : 2θ 's, interplaner spacings and intensities of various peaks observed in XRD of nickel and titanium substituted barium ferrite $\text{BaFe}_{12-2x}\text{Ni}_x\text{Ti}_x\text{O}_{19}$

x=0 Standard data				x=0 Observed		x=0.2 Observed	
$2\theta^\circ$	d(Å)	Relative intensity	h k l	d(Å)	Relative intensity	d (Å)	Relative Intensity
22.9	3.868	18	0 0 . 6	3.847	8	3.847	1
30.2	2.948	55	1 1 . 0	2.938	40	2.938	54
30.8	2.901	32	0 0 . 8	2.901	36	2.901	69
31.3	2.859	9	1 1 . 2	-	-	2.864	58
32.1	2.782	100	1 0 . 7	2.786	100	2.786	100
34.1	2.628	98	1 1 . 4	2.627	97	2.627	99
35.1	2.553	11	2 0 . 0	-	-	-	-
35.6	2.522	10	1 0 . 8	-	-	-	-
37.0	2.425	60	2 0 . 3	2.428	50	2.241	48
38.7	2.322	<1	0 0 . 10	-	-	-	-
39.1	2.303	4	1 0 . 9	-	-	-	-
40.3	2.237	29	2 0 . 5	2.231	35	2.236	29
42.4	2.131	18	2 0 . 6	2.130	23	2.130	27
42.8	2.113	3	1 0 . 10	-	-	-	-
46.4	1.949	9	1 0 . 11	1.947	9	-	-
46.9	1.934	<1	0 0 . 12	-	-	-	-
49.9	1.823	6	1 0 . 10	-	-	-	-
50.3	1.814	10	2 0 . 9	1.812	12	1.812	10
53.2	1.718	3	2 0 . 10	-	-	-	-
53.8	1.701	8	3 0 . 0	1.697	10	-	-
54.4	1.684	5	3 0 . 2	-	-	-	-
55.0	1.668	53	2 1 . 7	1.668	55	1.665	45
55.4	1.658	8	0 0 . 14	-	-	-	-
56.3	1.633	30	3 0 . 4	-	-	-	-
56.5	1.626	58	2 0 . 11	1.630	78	1.627	76
56.8	1.618	10	1 1 . 12	-	-	-	-
57.3	1.606	7	2 1 . 8	-	-	-	-
58.4	1.578	3	1 0 . 14	-	-	-	-
59.8	1.546	2	2 1 . 9	-	-	-	-
59.9	1.541	3	2 0 . 12	-	-	-	-
62.5	1.484	2	2 1 . 10	-	-	-	-
62.7	1.481	6	1 0 . 15	-	-	-	-
63.0	1.474	63	2 2 . 0	1.474	54	1.427	52
63.5	1.463	5	2 0 . 13	-	-	-	-
64.1	1.451	<1	0 0 . 16	-	-	-	-
65.5	1.424	3	2 1 . 11	-	-	1.424	<2
67.3	1.390	13	2 0 . 14	1.388	14	-	-
68.0	1.377	4	2 2 . 6	-	-	-	-
71.7	1.314	9	2 2 . 8	-	-	-	-
72.0	1.310	4	2 1 . 13	1.310	7	1.310	28
72.5	1.302	15	3 1 . 7	1.304	27	1.298	<1
74.1	1.278	3	3 0 . 12	-	-	-	-
75.4	1.259	6	4 0 . 3	-	-	-	-

Table 19 :2 θ 's, interplaner spacings and intensities of various peaks observed in XRD of nickel and titanium substituted barium ferrite BaFe_{12-2x}Ni_xTi_xO₁₉

x= 0 Standard data				x=0 Observed		x=0.4 Observed	
2 θ°	d(\AA)	Relative intensity	h k .l	d(\AA)	Relative intensity	d (\AA)	Relative Intensity
22.9	3.868	18	0 0 . 6	3.847	8	3.864	<10
30.2	2.948	55	1 1 . 0	2.938	40	2.947	48
30.8	2.901	32	0 0 . 8	2.901	36	-	-
31.3	2.859	9	1 1 . 2	-	-	-	-
32.1	2.782	100	1 0 . 7	2.786	100	2.786	91
34.1	2.628	98	1 1 . 4	2.627	97	2.627	100
35.1	2.553	11	2 0 . 0	-	-	-	-
35.6	2.522	10	1 0 . 8	-	-	-	-
37.0	2.425	60	2 0 . 3	2.428	50	2.248	44
38.7	2.322	<1	0 0 . 10	-	-	-	-
39.1	2.303	4	1 0 . 9	-	-	-	-
40.3	2.237	29	2 0 . 5	2.231	35	2.241	29
42.4	2.131	18	2 0 . 6	2.130	23	2.135	20
42.8	2.113	3	1 0 . 10	-	-	-	-
46.4	1.949	9	1 0 . 11	1.947	9	-	-
46.9	1.934	<1	0 0 . 12	-	-	-	-
49.9	1.823	6	1 0 . 10	-	-	-	-
50.3	1.814	10	2 0 . 9	1.812	12	1.816	<1
53.2	1.718	3	2 0 . 10	-	-	-	-
53.8	1.701	8	3 0 . 0	1.697	10	1.703	16
54.4	1.684	5	3 0 . 2	-	-	-	-
55.0	1.668	53	2 1 . 7	1.668	55	1.668	48
55.4	1.658	8	0 0 . 14	-	-	-	-
56.3	1.633	30	3 0 . 4	-	-	-	-
56.5	1.626	58	2 0 . 11	1.630	78	1.627	66
56.8	1.618	10	1 1 . 12	-	-	-	-
57.3	1.606	7	2 1 . 8	-	-	-	-
58.4	1.578	3	1 0 . 14	-	-	-	-
59.8	1.546	2	2 1 . 9	-	-	1.545	3
59.9	1.541	3	2 0 . 12	-	-	-	-
62.5	1.484	2	2 1 . 10	-	-	-	-
62.7	1.481	6	1 0 . 15	-	-	-	-
63.0	1.474	63	2 2 . 0	1.474	54	1.474	56
63.5	1.463	5	2 0 . 13	-	-	-	-
64.1	1.451	<1	0 0 . 16	-	-	-	-
65.5	1.424	3	2 1 . 11	-	-	-	-
67.3	1.390	13	2 0 . 14	1.388	14	1.390	14
68.0	1.377	4	2 2 . 6	-	-	1.377	9
71.7	1.314	9	2 2 . 8	-	-	1.314	6
72.0	1.310	4	2 1 . 13	1.310	7	-	-
72.5	1.302	15	3 1 . 7	1.304	27	1.303	20
74.1	1.278	3	3 0 . 12	-	-	-	-
75.4	1.259	6	4 0 . 3	-	-	1.258	5

Table 20 : 2θ 's, interplaner spacings and intensities of various peaks observed in XRD of nickel and titanium substituted barium ferrite $\text{BaFe}_{12-2x}\text{Ni}_x\text{Ti}_x\text{O}_{19}$

$x=0$ Standard data				$x=0$ Observed		$x=0.6$ Observed	
$2\theta^\circ$	$d(\text{\AA})$	Relative intensity	h k l	$d(\text{\AA})$	Relative intensity	$d(\text{\AA})$	Relative Intensity
22.9	3.868	18	0 0 . 6	3.847	8	3.831	8
30.2	2.948	55	1 1 . 0	2.938	40	2.938	48
30.8	2.901	32	0 0 . 8	2.901	36	-	-
31.3	2.859	9	1 1 . 2	-	-	-	-
32.1	2.782	100	1 0 . 7	2.786	100	2.769	100
34.1	2.628	98	1 1 . 4	2.627	97	2.620	92
35.1	2.553	11	2 0 . 0	-	-	-	-
35.6	2.522	10	1 0 . 8	-	-	-	-
37.0	2.425	60	2 0 . 3	2.428	50	2.415	42
38.7	2.322	<1	0 0 . 10	-	-	-	-
39.1	2.303	4	1 0 . 9	-	-	-	-
40.3	2.237	29	2 0 . 5	2.231	35	2.231	32
42.4	2.131	18	2 0 . 6	2.130	23	2.130	21
42.8	2.113	3	1 0 . 10	-	-	-	-
46.4	1.949	9	1 0 . 11	1.947	9	1.947	10
46.9	1.934	<1	0 0 . 12	-	-	-	-
49.9	1.823	6	1 0 . 10	-	-	-	-
50.3	1.814	10	2 0 . 9	1.812	12	1.806	12
53.2	1.718	3	2 0 . 10	-	-	-	-
53.8	1.701	8	3 0 . 0	1.697	10	1.670	16
54.4	1.684	5	3 0 . 2	-	-	-	-
55.0	1.668	53	2 1 . 7	1.668	55	1.665	49
55.4	1.658	8	0 0 . 14	-	-	-	-
56.3	1.633	30	3 0 . 4	-	-	-	-
56.5	1.626	58	2 0 . 11	1.630	78	1.622	75
56.8	1.618	10	1 1 . 12	-	-	-	-
57.3	1.606	7	2 1 . 8	-	-	-	-
58.4	1.578	3	1 0 . 14	-	-	-	-
59.8	1.546	2	2 1 . 9	-	-	-	-
59.9	1.541	3	2 0 . 12	-	-	1.538	8
62.5	1.484	2	2 1 . 10	-	-	-	-
62.7	1.481	6	1 0 . 15	-	-	-	-
63.0	1.474	63	2 2 . 0	1.474	54	1.470	58
63.5	1.463	5	2 0 . 13	-	-	-	-
64.1	1.451	<1	0 0 . 16	-	-	-	-
65.5	1.424	3	2 1 . 11	-	-	-	-
67.3	1.390	13	2 0 . 14	1.388	14	1.388	12
68.0	1.377	4	2 2 . 6	-	-	-	-
71.7	1.314	9	2 2 . 8	-	-	-	-
72.0	1.310	4	2 1 . 13	1.310	7	-	-
72.5	1.302	15	3 1 . 7	1.304	27	1.300	16
74.1	1.278	3	3 0 . 12	-	-	-	-
75.4	1.259	6	4 0 . 3	-	-	-	-

Table 21 : 2θ 's, interplaner spacings and intensities of various peaks observed in XRD of nickel and titanium substituted barium ferrite $\text{BaFe}_{12-2x}\text{Ni}_x\text{Ti}_x\text{O}_{19}$

x= 0 Standard data				x=0 Observed		x=0.8 Observed	
$2\theta^\circ$	$d(\text{\AA})$	Relative intensity	h k .l	$d(\text{\AA})$	Relative intensity	$d(\text{\AA})$	Relative Intensity
22.9	3.868	18	0 0 . 6	3.847	8	-	-
30.2	2.948	55	1 1 . 0	2.938	40	2.938	42
30.8	2.901	32	0 0 . 8	2.901	36	-	-
31.3	2.859	9	1 1 . 2	-	-	-	-
32.1	2.782	100	1 0 . 7	2.786	100	2.778	100
34.1	2.628	98	1 1 . 4	2.627	97	2.620	91
35.1	2.553	11	2 0 . 0	-	-	-	-
35.6	2.522	10	1 0 . 8	-	-	-	-
37.0	2.425	60	2 0 . 3	2.428	50	2.409	42
38.7	2.322	<1	0 0 . 10	-	-	-	-
39.1	2.303	4	1 0 . 9	-	-	-	-
40.3	2.237	29	2 0 . 5	2.231	35	2.225	34
42.4	2.131	18	2 0 . 6	2.130	23	-	-
42.8	2.113	3	1 0 . 10	-	-	2.120	24
46.4	1.949	9	1 0 . 11	1.947	9	-	-
46.9	1.934	<1	0 0 . 12	-	-	-	-
49.9	1.823	6	1 0 . 10	-	-	-	-
50.3	1.814	10	2 0 . 9	1.812	12	1.806	<1
53.2	1.718	3	2 0 . 10	-	-	-	-
53.8	1.701	8	3 0 . 0	1.697	10	-	-
54.4	1.684	5	3 0 . 2	-	-	-	-
55.0	1.668	53	2 1 . 7	1.668	55	-	-
55.4	1.658	8	0 0 . 14	-	-	1.660	40
56.3	1.633	30	3 0 . 4	-	-	-	-
56.5	1.626	58	2 0 . 11	1.630	78	1.662	97
56.8	1.618	10	1 1 . 12	-	-	-	-
57.3	1.606	7	2 1 . 8	-	-	1.607	<1
58.4	1.578	3	1 0 . 14	-	-	-	-
59.8	1.546	2	2 1 . 9	-	-	-	-
59.9	1.541	3	2 0 . 12	-	-	-	-
62.5	1.484	2	2 1 . 10	-	-	-	-
62.7	1.481	6	1 0 . 15	-	-	-	-
63.0	1.474	63	2 2 . 0	1.474	54	1.470	76
63.5	1.463	5	2 0 . 13	-	-	-	-
64.1	1.451	<1	0 0 . 16	-	-	-	-
65.5	1.424	3	2 1 . 11	-	-	-	-
67.3	1.390	13	2 0 . 14	1.388	14	1.386	21
68.0	1.377	4	2 2 . 6	-	-	-	-
71.7	1.314	9	2 2 . 8	-	-	-	-
72.0	1.310	4	2 1 . 13	1.310	7	-	-
72.5	1.302	15	3 1 . 7	1.304	27	1.300	23
74.1	1.278	3	3 0 . 12	-	-	-	-
75.4	1.259	6	4 0 . 3	-	-	1.257	<1

Table 22 : 2θ 's, interplaner spacings and intensities of various peaks observed in XRD of nickel and titanium substituted barium ferrite $\text{BaFe}_{12-2x}\text{Ni}_x\text{Ti}_x\text{O}_{19}$

x= 0 Standard data				x=0 Observed		x=1.0 Observed	
$2\theta^\circ$	d(Å)	Relative intensity	h k .l	d(Å)	Relative intensity	d (Å)	Relative Intensity
22.9	3.868	18	0 0 . 6	3.847	8	-	-
30.2	2.948	55	1 1 . 0	2.938	40	2.938	47
30.8	2.901	32	0 0 . 8	2.901	36	-	-
31.3	2.859	9	1 1 . 2	-	-	-	-
32.1	2.782	100	1 0 . 7	2.786	100	2.786	97
34.1	2.628	98	1 1 . 4	2.627	97	2.627	100
35.1	2.553	11	2 0 . 0	-	-	-	-
35.6	2.522	10	1 0 . 8	-	-	2.526	16
37.0	2.425	60	2 0 . 3	2.428	50	2.420	57
38.7	2.322	<1	0 0 . 10	-	-	-	-
39.1	2.303	4	1 0 . 9	-	-	-	-
40.3	2.237	29	2 0 . 5	2.231	35	2.231	35
42.4	2.131	18	2 0 . 6	2.130	23	-	-
42.8	2.113	3	1 0 . 10	-	-	2.116	21
46.4	1.949	9	1 0 . 11	1.947	9	-	-
46.9	1.934	<1	0 0 . 12	-	-	-	-
49.9	1.823	6	1 0 . 10	-	-	-	-
50.3	1.814	10	2 0 . 9	1.812	12	1.812	18
53.2	1.718	3	2 0 . 10	-	-	-	-
53.8	1.701	8	3 0 . 0	1.697	10	1.697	10
54.4	1.684	5	3 0 . 2	-	-	-	-
55.0	1.668	53	2 1 . 7	1.668	55	1.665	61
55.4	1.658	8	0 0 . 14	-	-	-	-
56.3	1.633	30	3 0 . 4	-	-	-	-
56.5	1.626	58	2 0 . 11	1.630	78	1.625	97
56.8	1.618	10	1 1 . 12	-	-	-	-
57.3	1.606	7	2 1 . 8	-	-	-	-
58.4	1.578	3	1 0 . 14	-	-	-	-
59.8	1.546	2	2 1 . 9	-	-	-	-
59.9	1.541	3	2 0 . 12	-	-	-	-
62.5	1.484	2	2 1 . 10	-	-	-	-
62.7	1.481	6	1 0 . 15	-	-	-	-
63.0	1.474	63	2 2 . 0	1.474	54	1.427	81
63.5	1.463	5	2 0 . 13	-	-	-	-
64.1	1.451	<1	0 0 . 16	-	-	-	-
65.5	1.424	3	2 1 . 11	-	-	-	-
67.3	1.390	13	2 0 . 14	1.388	14	1.388	13
68.0	1.377	4	2 2 . 6	-	-	-	-
71.7	1.314	9	2 2 . 8	-	-	-	-
72.0	1.310	4	2 1 . 13	1.310	7	1.310	13
72.5	1.302	15	3 1 . 7	1.304	27	1.300	29
74.1	1.278	3	3 0 . 12	-	-	-	-
75.4	1.259	6	4 0 . 3	-	-	-	-

tures with increase of Ni-Ti content. The value of Curie temperature (T_c) has been determined by interaction of tangent, drawn at largest slope point on magnetization vs. temperature curve, with abscissa. The drastic drop in Curie temperature exhibited by $\text{BaFe}_{12-2x}\text{Ni}_x\text{Ti}_x\text{O}_{19}$ is due to Ni^{2+} and Ti^{4+} insertion. As substitution of non-magnetic ions increases, the strength of super exchange interaction decreases and cause drop in the value of Curie temperature [29] .

Table 23 : Saturation magnetization and coercivity of different nickel and titanium containing barium ferrite $\text{BaFe}_{12-2x}\text{Ni}_x\text{Ti}_x\text{O}_{19}$

Amount of substitution x	Saturation Magnetization (emu/g)	Coercivity H_c (Oe)	Curie Temperature T_c ($^{\circ}\text{C}$)
0.0	59.3 ± 0.1	4300	458
0.2	52.0 ± 0.0	3000	345
0.4	54.3 ± 0.1	2453	---
0.6	55.5 ± 0.1	2130	---
0.8	53.5 ± 0.1	1900	---
1.0	58.4 ± 0.1	1301	340

3.2.3 Mossbauer spectroscopic analysis

The Mossbauer spectra of $\text{BaFe}_{12-2x}\text{Ni}_x\text{Ti}_x\text{O}_{19}$ with $0 \leq x \leq 1.0$ at room temperature are shown in Figs 24 and 25. These were fitted with various sextet subpatterns corresponding to five different sites $4f_{iv}$, $4f_{vi}$, 2a, 2b and 12k of pure barium ferrite and others possibly developing due to Ni-Ti substitution. The values corresponding to hyperfine field and relative spectral area for $\text{BaFe}_{12-2x}\text{Ni}_x\text{Ti}_x\text{O}_{19}$ with $0 \leq x \leq 1.0$ are given in Table 24. The variations of hyperfine field and the relative spectral area are shown

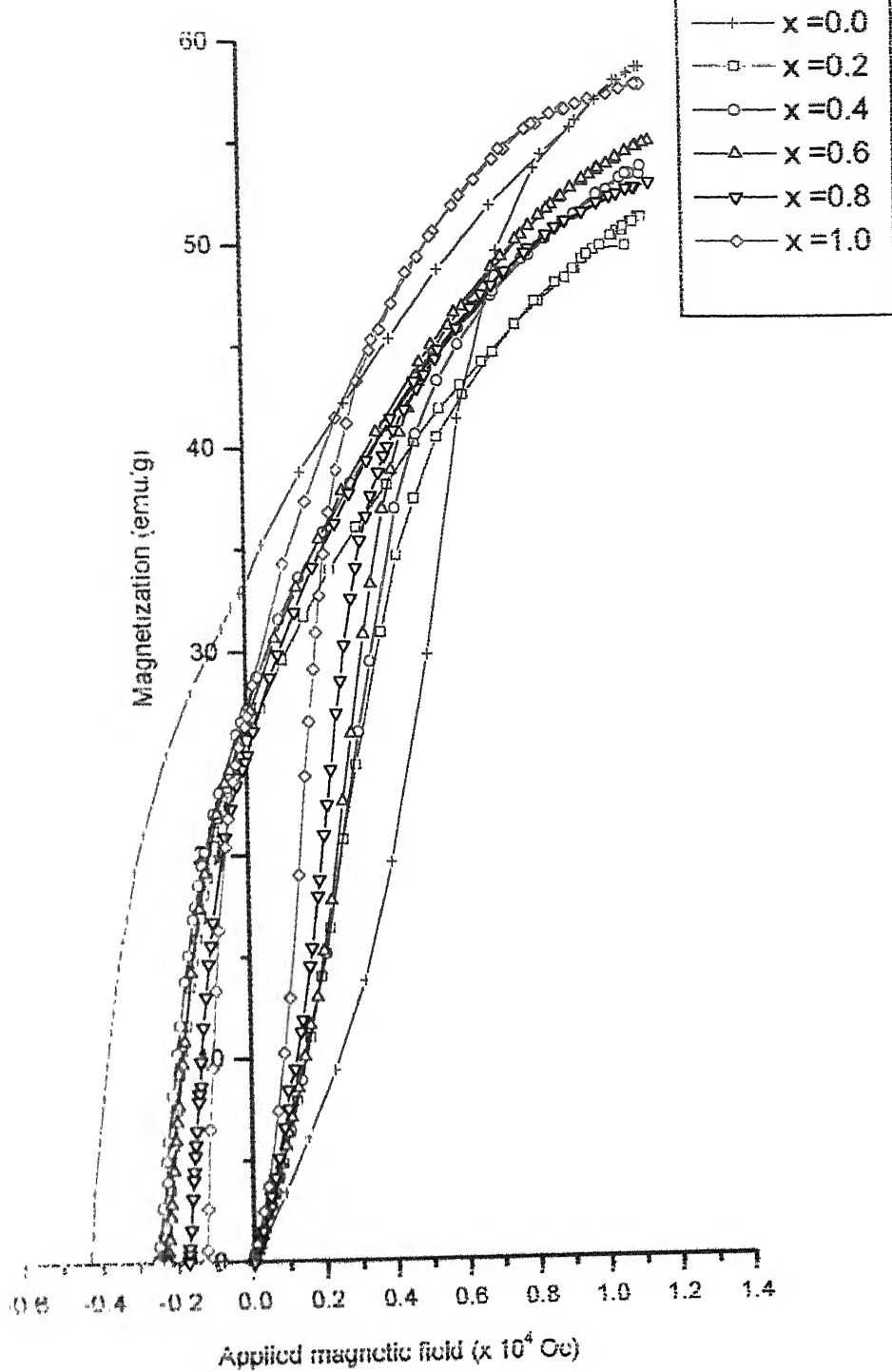


Fig. 20. Magnetization versus applied field curve for nickel and titanium substituted barium ferrite $\text{BaFe}_{12-2x}\text{Ni}_x\text{Ti}_x\text{O}_{19}$

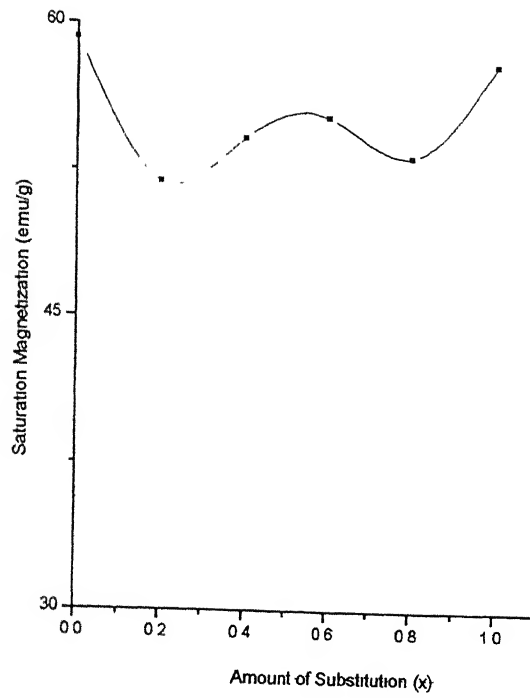


Fig. 21 : Saturation magnetization of $\text{BaFe}_{12-2x}\text{Ni}_x\text{Ti}_x\text{O}_{19}$ as a function of x

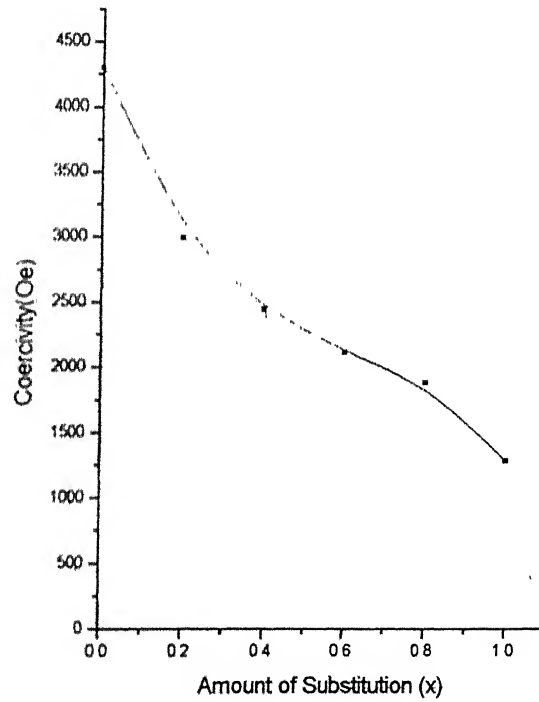


Fig. 22: Coercivity of $\text{BaFe}_{12-2x}\text{Ni}_x\text{Ti}_x\text{O}_{19}$ as a function of x

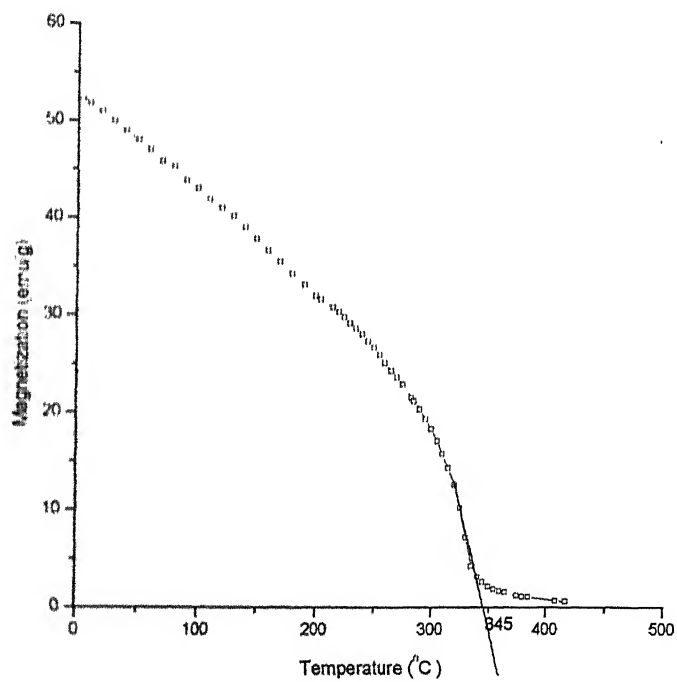
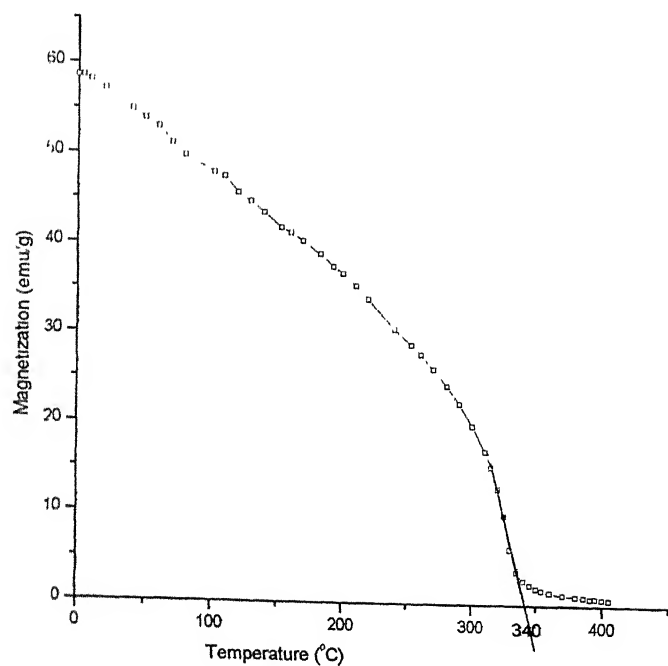


Fig. 23: Variation of magnetization with temperature of barium ferrite of composition $\text{BaFe}_{12-2x}\text{Ni}_x\text{Ti}_x\text{O}_{19}$ with (a) $x=0.2$ (b) $x=1.0$

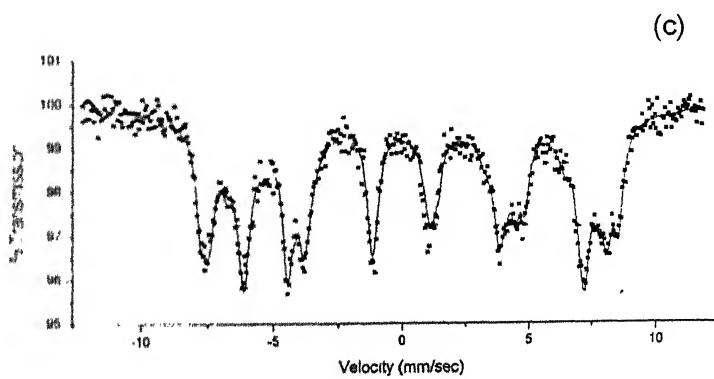
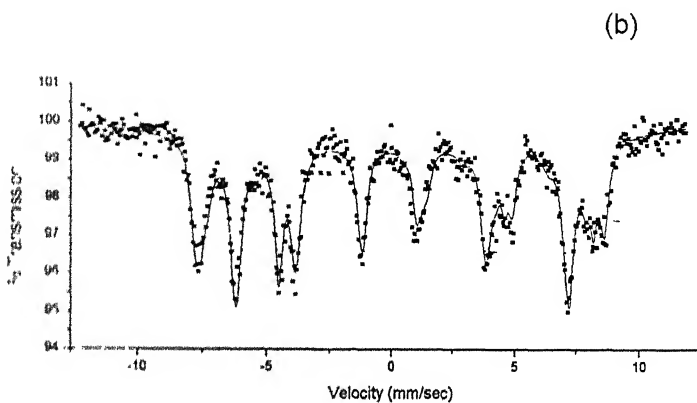
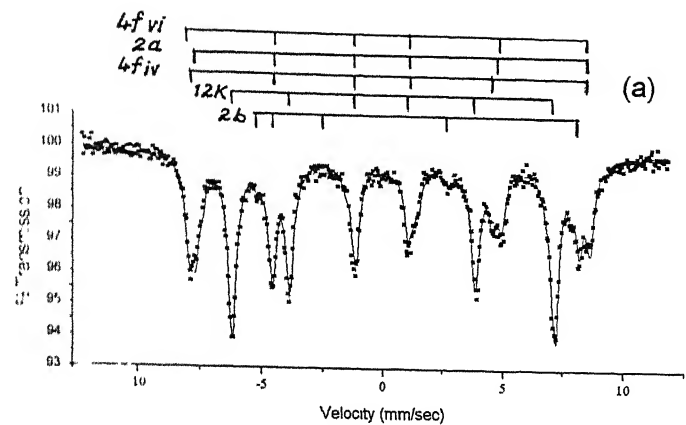


Fig 24: Mossbauer spectra of barium ferrite of composition $\text{BaFe}_{12-2x}\text{Ni}_x\text{Ti}_x\text{O}_{19-x/2}$ with (a) $x=0.0$ (b) $x=0.2$ (c) $x=0.4$

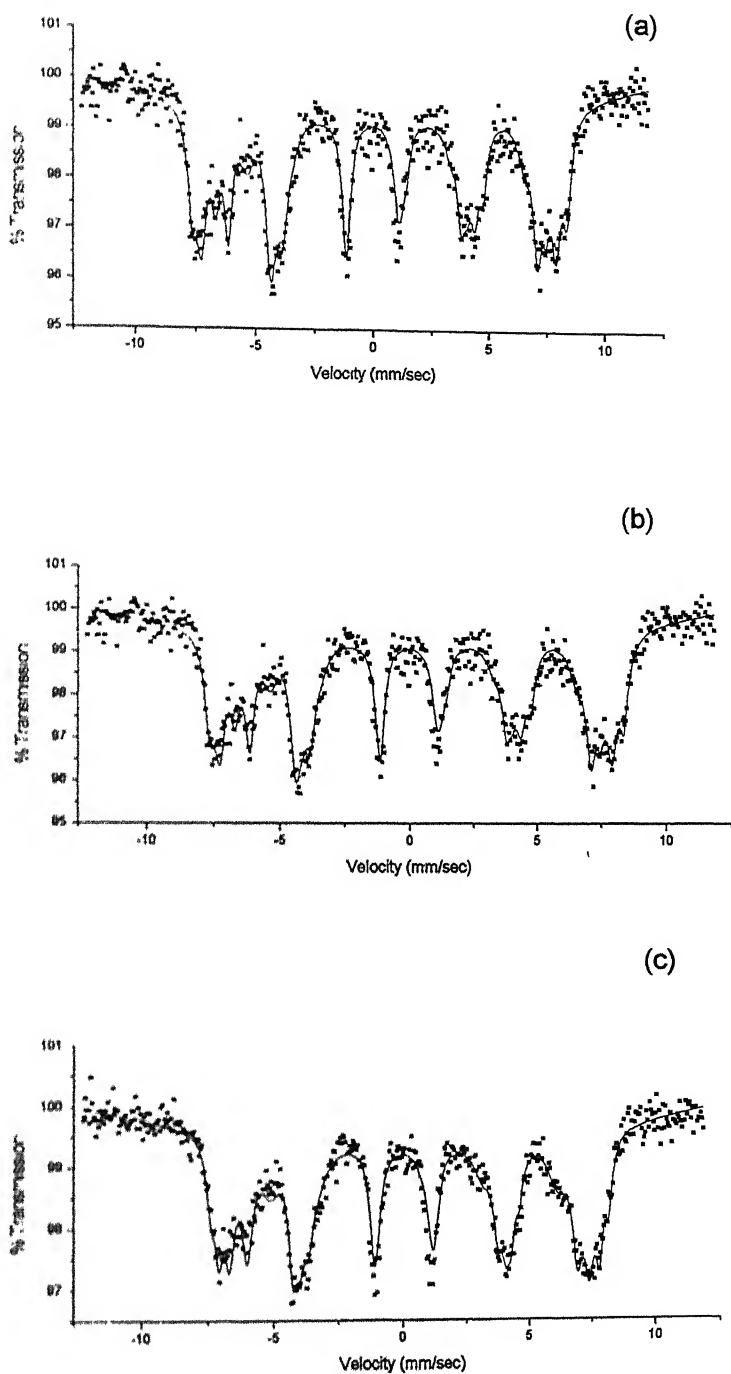


Fig 25: Mossbauer spectra of barium ferrite of composition $\text{BaFe}_{12-2x}\text{Ni}_x\text{Ti}_x\text{O}_{19-x/2}$ with (a) $x=0.6$ (b) $x=0.8$ (c) $x=1.0$

Table 24 : Relative spectral areas and hyperfine (Internal magnetic) fields of different crystallographic sites of barium ferrite of composition $\text{BaFe}_{12-2x}\text{Ni}_x\text{Ti}_x\text{O}_{19}$.

Amount of substit ion (x)	Site(4f _a)			Site(2a)			Site(4f _c)			Site(12k)			Site (2b)			New site			New site		
	Area (%)	Int. Mag Field (kOe)		Area (%)	Int. Mag Field (kOe)		Area (%)	Int. Mag Field (kOe)		Area (%)	Int. Mag Field (kOe)		Area (%)	Int. Mag Field (kOe)		Area (%)	Int. Mag Field (kOe)		Area (%)	Int. Mag Field (kOe)	
0	16.39	517		4.00	505		23.32	490		51.88	413		4.58	404		-	-		-	-	
0.2	20.59	511		1.46	506		22.22	486		46.04	418		-	-		9.86	409		-	-	
0.4	18.37	509		-	-		26.42	483		45.48	418		-	-		2.54	407		7.18	373	
0.6	19.44	499		-	-		33.84	469		32.91	417		-	-		2.22	403		11.59	367	
0.8	25.18	490		-	-		27.38	459		25.01	412		-	-		11.86	407		10.15	395	
1.0	28.12	472		-	-		23.38	443		23.46	404		-	-		-	-		14.89	325	

in Figs. 26 and 27. The relative spectral areas for 2a, 12k and 2b sites decrease while for $4f_{iv}$ and $4f_{vi}$ sites vary randomly with increase of Ni-Ti substitution. Hyperfine field decreases for crystallographic sites $4f_{iv}$, $4f_{vi}$, 2a and 2b but varies randomly for the 12k. Such a variation in hyperfine field is perhaps due to the change occurring in the nature of cations in surrounding of respective of locations.

Nickel ions invariably occupy octahedral sites [29]. The titanium ion also prefers octahedral site because of large volume available and possibility of accommodating distortion of associated polyhedra. Moreover, the outer electronic structure of Ti^{4+} ion is less compressible than that of other ions with full- or half- filled d orbital. Thus, Ti^{4+} strongly prefers octahedral co-ordination for stability as well. Since both the Ni^{2+} and Ti^{4+} ions prefer the same site, there is competition between the two. As the number of sites is limited, the occupancy preference forces the emergence of secondary phase as well [29].

The spectral area decreases for the 12k, 2a and 2b sites, indicating preferential substitution there. The sharp decrease in areas of the crystallographic 12k and 2a octahedral sites – conform their occupation with Ni^{2+} and Ti^{4+} ions. Ni-Ti substitution on 12k sites leads to the decrease in saturation magnetization with temperature too. The isomer shift and quadrupole splitting for the sextet corresponding to the 2b site are larger as compared to other sites. Fe^{3+} ions in the trigonal 2b and octrahedral $4f_{vi}$ sites are responsible for the uniaxial anisotropy of barium ferrite [17]. The magnetic anisotropy decreases by making a substitute of less

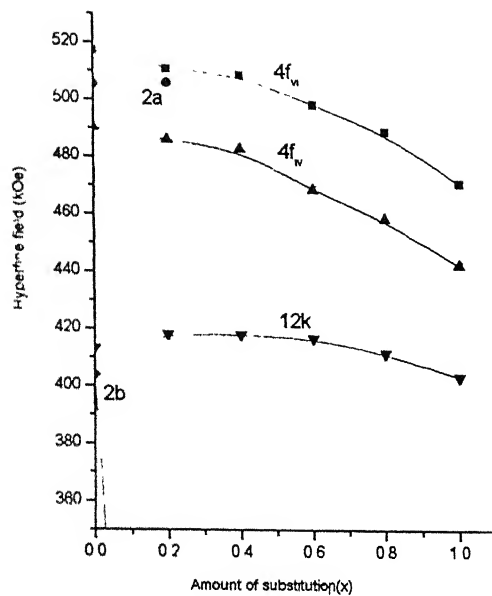


Fig 26: Hyperfine field for different sites in $\text{BaFe}_{12-2x}\text{Ni}_x\text{Ti}_x\text{O}_{19}$ at room temperature versus amount of substitution

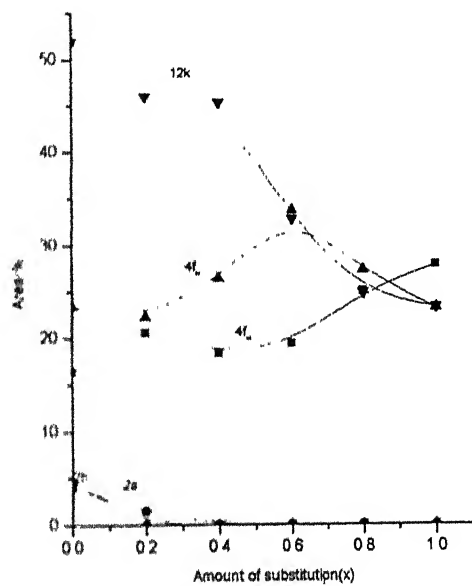


Fig 27: Sextet area(normalized to 100%)of different sites in $\text{BaFe}_{12-2x}\text{Ni}_x\text{Ti}_x\text{O}_{19}$ versus substitution

magnetic or non-magnetic ions. Also, the magnetic moment of nickel ($=0.60\mu_B$ per atom) is smaller than that of iron ($=2.20\mu_B$ per atom). Ni-Ti substitution on the 2b site (where Fe^{3+} has spin up) must result in decrease in magnetic moment and, in turn, magnetic anisotropy. This means coercivity should also decrease correspondingly.

Saturation magnetization can be increased when non-magnetic or less magnetic ions than Fe^{3+} occupy spin down sites (i.e., f_{iv} , f_{vi}). On the other hand, saturation magnetization can be decreased by non-magnetic or less magnetic ions (with spin up) occupying 12k, 2a and 2b sites. In $\text{BaFe}_{12-2x}\text{Ni}_x\text{Ti}_x\text{O}_{19}$ samples, the saturation magnetization varies randomly with the increase of substitution. Also, Mossbauer spectra show random changes in spectral areas for $4f_{vi}$ and $4f_{iv}$ sites with definite decrease in areas of 12k, 2a and 2b sites. As f_{vi} and f_{iv} sites are known to have spin down Fe^{3+} , their substitution by Ni^{2+} and Ti^{4+} ions can lead to increase in the overall saturation magnetization.

The two new crystallographic sites found in Mossbauer data may be due to the competition between Ni^{2+} and Ti^{4+} ions for occupying the octahedral sites. In yet another fitting of Mossbauer spectra, 2b site is found to be empty altogether with a new filled site corresponding to hyperfine field of 375kOe with low chi square value in pure and modified barium hexaferrite samples. This is perhaps arising due to difference in pH used during the synthesis, i.e., 6.5 instead of 4.0, as 2b site is normally occupied in pure barium ferrite. The present data can not resolve this discrepancy.

3.3 Microstructure and general discussion

Fig. 28 shows a few typical microstructures of pure and Ni^{2+} and Ni^{2+} - Ti^{4+} substituted barium ferrites as observed in a scanning electron microscope (JEOL 840A) operated at 15kV in the secondary electron mode (SE) mode. In all, particles of sub-micron size of no particular shape are clearly visible. Also, effects of agglomeration can be noticed at several places. All samples however, exhibited similar microstructures and therefore no correlation was possible with the variation in compositions.

The barium ferrites of compositions $\text{BaFe}_{12-x}\text{Co}_x\text{O}_{19-x/2}$ with $0 \leq x \leq 1.6$ and $\text{BaFe}_{12-2x}\text{Co}_x\text{Ti}_x\text{O}_{19}$ with $0 \leq x \leq 1.0$, synthesized by auto-ignition method itself, are discussed in earlier reports [13, 30]. Their characteristics are summarized in Tables 25 and 26 for comparing the results arrived at in the present investigation with nickel and nickel-titanium substituted compounds. It seems that nickel substitution has greater bearing on the saturation magnetization in comparison to cobalt in barium ferrite. The saturation magnetization of $\text{BaFe}_{12-x}\text{Ni}_x\text{O}_{19-x/2}$ samples decreases continuously with the nickel content whereas it remains nearly constant in case of cobalt substituted compounds. Also, the decrease in coercivity is more for nickel substituted barium ferrites. These results suggest that partial substitution of iron by nickel is more effective than cobalt in reducing the magnetic anisotropy in barium ferrite. Though Curie temperature increases in both the cases with increase in the level of substitution and increase is small for of $\text{BaFe}_{12-x}\text{Ni}_x\text{O}_{19-x/2}$ compounds, yet, its value remains suitable for magnetic recording applications. The XRD patterns show the existence of a single-phase up to $x=1.4$ and a secondary phase in case of $\text{BaFe}_{12-x}\text{Co}_x\text{O}_{19-x/2}$

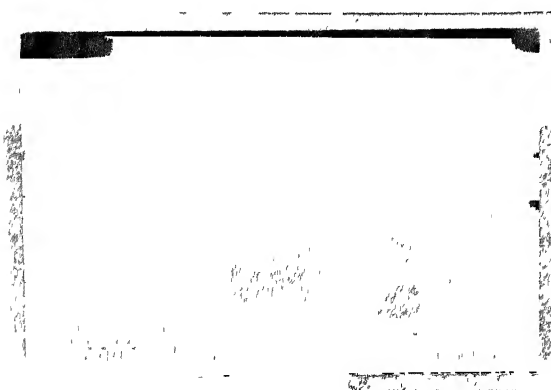
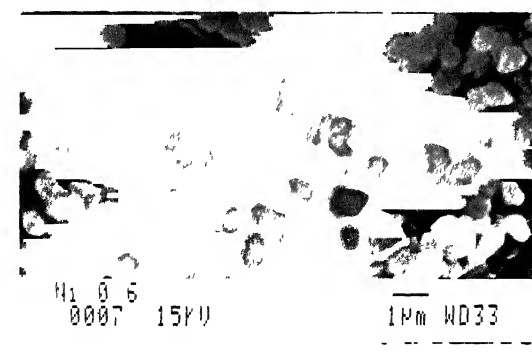
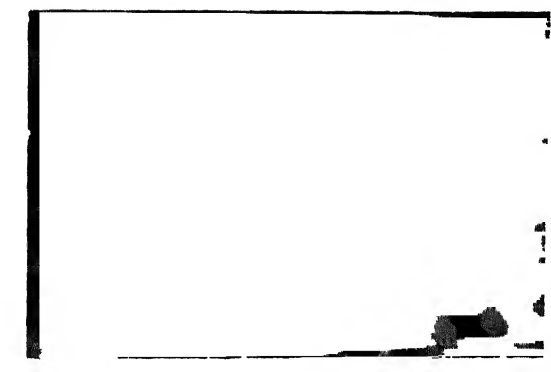


Fig. 28. Scanning electron micrographs of (a) $\text{BaFe}_{12}\text{O}_{19}$, (b) $\text{BaFe}_{12x}\text{Ni}_x\text{O}_{19-x/2}$ with $x=1.2$ and (c) $\text{BaFe}_{12-2x}\text{Ni}_x\text{Ti}_x\text{O}_{19}$ with $x=1.2$ compounds

Table 25 : Comparison of magnetic properties of nickel and cobalt substituted barium hexaferrites.

	BaFe _{12-x} Ni _x O _{19-x/2}				BaFe _{12-x} Co _x O _{19-x/2}			
	Preparation condition pH = 6.5 Calcination temperature = 1000° C				Preparation condition pH = 4 Calcination temperature = 1100			
Amount of Substitution (x)	Saturation Magnetization M _s (emu/g)	Coercivity H _c (Oe)	Curie Temperature T _c (°C)		Saturation Magnetization (M _s) (emu/g)	Coercivity H _c (Oe)	Curie Temperature T _c (°C)	
0	59.3	4300	458		58.7	4223	481	
0.2	55.8	3403	---		---	-----	483	
0.4	----	---	---		59.9	3607	-----	
0.6	54.9	2911	463		---	---	487	
0.8	----	---	---		60.7	3119	---	
1.0	50.1	2761	466		61.2	2816	492	
1.2	48.8	2308	---		59.2	2639	495	
1.4	48.1	2074	474		---	---	499	
1.6	43.4	1379	---		54.2	2082	506	

Table 26 : Comparison of magnetic properties of nickel-titanium and cobalt-titanium substituted barium hexaferrites.

	BaFe _{12-2x} Ni _x Ti _x O ₁₉				BaFe _{12-2x} Co _x Ti _x O ₁₉			
	Preparation condition pH = 6				Preparation condition pH = 4			
	Calcination temperature = 1000° C				Calcination temperature = 1100			
Amount of Substitution (x)	Saturation Magnetization M _s (emu/g)	Coercivity H _c (Oe)	Curie Temperature T _c (°C)		Saturation Magnetization (M _s) (emu/g)	Coercivity H _c (Oe)	Curie Temperature T _c (°C)	
0	59.3	4300	458		58.8	4223	481	
0.2	52.0	3000	345		61.2	2676	---	
0.4	54.3	2453	---		61.1	1600	448	
0.6	55.5	2130	---		60.5	1110	430	
0.8	53.5	1900	---		58.8	786	---	
1.0	58.4	1301	340		56.2	407	392	

for $x > 1.4$. In contrast, secondary phase begins to appear at the substitution level of $x = 0.8$ in nickel substituted compounds. Efforts are needed to suppress the formation of secondary phase(s) so that a single-phase material of low coercivity can be synthesized for magnetic recording applications.

For both the Co-Ti and Ni-Ti substituted barium hexaferrites, the saturation magnetization remains nearly constant (Table 26). But, the decrease in coercivity is less for Ni-Ti substituted barium ferrite. So, by increasing substitution level, it is possible to decrease coercivity in a controlled manner with Ni-Ti substituted ferrites. XRD patterns show the existence of single phase in both types of hexaferrite up to $x = 1.0$. Further, Curie temperature decreases to a large degree with with partial substitution of iron by nickel than cobalt in barium ferrites.

Gornert, Sinn, Schuppel, Pfeiffer, Rosler, Schubert, Jurisch and Sellger [22] have prepared $\text{BaFe}_{12-2x}\text{Co}_x\text{Ti}_x\text{O}_{19}$ with $0 \leq x \leq 0.9$ by glass crystallization method. According to them, selection of x and crystallization temperature appropriately, barium ferrite particles with a narrow size distribution and desired magnetic properties can be produced in bulk for magnetic recording applications. For example, at $x = 0.9$, coercivity of glass flakes heated at 850°C for 10h corresponds to 400 Oe.

Kubo, Ido, Yokoyama and Koike [24] have synthesized cobalt substituted ferrites of composition $\text{BaFe}_{12-2x}\text{Co}_x\text{Ti}_x\text{O}_{19}$ with $x = 0, 0.5$ and 0.85 by glass crystallization method and observed decrease of saturation magnetization with decrease in particle size. This result was explained by assuming the existence of a few Angstrom thick non-magnetic layer on

the surface of particles and corresponding decrease in the magnetic volume fraction. Further, the coercivity variation with the mean particle size was found to follow either super-paramagnetism theory or multi-domain nucleation mechanism.

Chen, Sorensen, Klabunde, Hadjipanayis, Devlin and Kostikas [20] produced MnFe_2O_4 by aqueous phase co-precipitation method and showed decrease of both the Curie temperature and saturation magnetization with decrease in the mean particle size.

Turilli, Licci, Rinaldi and Deriu [23] have synthesized Mn-Ti substituted ferrites of composition $\text{BaFe}_{12-2x}\text{Mn}_x\text{Ti}_x\text{O}_{19}$ ($0 < x < 2$) by mixing stoichiometric oxides and carbonates using a ceramic route and found saturation magnetization to remain unaffected up to $x=0.4$. The large perturbation of magnetic order was, however, observed in samples corresponding to $x > 0.5$. This was attributed to the preferential occupation of 12k sites by both Mn^{2+} and Ti^{4+} ions in magneto-plumbite structure.

Turilli, Licci, Paoluzi and Besagni [31] used metallorganic precursor method to prepare $\text{Sr}(\text{NiTi})_x\text{Fe}_{12-2x}\text{O}_{19}$ hexaferrite with $0.3 \leq x \leq 0.9$. They found 1) nickel to be quite effective in reducing the magneto-crystalline anisotropy (or coercivity), e.g., H_c value decreases from 16000 Oe for $x=0$ to 7700 Oe for $x=0.9$. In contrast, Co-Ti substitution reduces the coercivity only to 11200 Oe for $x=0.9$, 2) decrease in the rate of formation of hexagonal phase at a fixed reaction temperature (T_r) with rise in Ni-Ti content, and 3) formation of single domain particles up to T_r of 1000°C .

Rane, Bahadur, Kulkarni and Date [29] adopted the citrate gel route to synthesize $\text{BaFe}_{12-2x}\text{Ni}_x\text{Zr}_x\text{O}_{19}$ compounds with $0.1 \leq x \leq 1.1$ and observed substantial decrease in coercivity with increase in x , i.e., from 3240 Oe to 180 Oe when x increases from 0.1 to 1.1. Further, Ni-Zr substituted barium ferrites are shown to be superior to Co-Ti substituted compounds for magnetic recording applications.

In conclusion by adjusting the amount of Ni^{2+} and Ti^{4+} ions (i.e., the value of x), it is possible to obtain $\text{BaFe}_{12-2x}\text{Ni}_x\text{Ti}_x\text{O}_{19}$ compounds of desirable characteristics for magnetic recording application, e.g., products with $x=0.2-1.0$ exhibit coercivity and saturation magnetization in the range of 3000-1301 Oe and 52-58.4 emu/g.

Chapter 4

CONCLUSIONS

- 1 Nickel and nickel-titanium substituted barium ferrites of composition $\text{BaFe}_{12-x}\text{Ni}_x\text{O}_{19-x/2}$ with $0 \leq x \leq 1.6$ and $\text{BaFe}_{12-2x}\text{Ni}_x\text{Ti}_x\text{O}_{19}$ with $0 \leq x \leq 1.0$ can be successfully synthesized by auto-ignition method with characteristics suitable for high density information storage applications.
- 2 $\text{BaFe}_{12-x}\text{Ni}_x\text{O}_{19-x/2}$ maintains magneto-plumbite structure up to $x=0.6$ at least but exhibits another phase of composition NiFe_2O_4 progressively in increasing amount with rise in nickel content (x).

Nickel substitution (x) causes continuous decrease in coercivity (H_c) and saturation magnetization (M_s) of $\text{BaFe}_{12-x}\text{Ni}_x\text{O}_{19-x/2}$. e.g., H_c and M_s values 4300 and 1379 Oe, and 59.3 and 43.4 emu/g for $x=0$ and 1.6, respectively. But, Curie temperature (T_c) increases with x and corresponds to has value of 458°C and 474°C for $x=0$ and 1.4, respectively.

Mossbauer spectra suggest that nickel ions occupy 12k and 2b sites preferentially and randomly $4f_{vi}$, $4f_{iv}$ and/or 2a sites with increase of nickel content.

- 3 Nickel-titanium substituted barium hexaferrites of composition $\text{BaFe}_{12-2x}\text{Ni}_x\text{Ti}_x\text{O}_{19}$ with $0 \leq x \leq 1.0$ exhibit hexagonal structure

(magneto-plumbite type) with lattice parameter $a=5.867\pm0.001$ Å and $c=23.310\pm0.001$ Å.

Coercivity (H_c) decreases steadily from 4300 Oe to 1301 Oe as Ni-Ti content (x) increases from x=0 to 1.0. The saturation magnetization varies randomly but lie in the range 52-59.3 emu/g for compositions $0\leq x\leq 1.0$. Curie temperature drops drastically and corresponds to 458 °C and 340° C for x=0 and 1.0, respectively.

Mossbauer spectra indicate that Ni^{2+} and Ti^{4+} ions occupy preferentially 12k, 2a and 2b crystallographic sites as their relative spectral areas decrease sharply with the increase in level of substitution.

- 4 By adjusting the amount of Ni^{2+} and Ti^{4+} ions (i.e., the value of x), it is possible to obtain $BaFe_{12-2x}Ni_xTi_xO_{19}$ compounds of desirable characteristics for information storage application, e.g., products with x=0.2-1.0 exhibit coercivity and saturation magnetization in the range of 3000-1301Oe and 52-58.4 emu/g.

REFERENCES

1. M.P Sharrock, “ *Particulate magnetic recording media: a review*”, IEEE Trans. on Magnetics, **25**, 4374-4389 (1989).
2. J . C Mallinson, “ The foundation of magnetic Recording”, Academic press, San Diego, p5, CA (1987).
3. M.P.Sharrock and L.W.Carlson, "*The application of barium ferrite particles in advanced recording media* ", IEEE Trans. on Magnetics, **31**, 2871-2876 (1995).
4. R. Wood, “*Magnetic megabits*”, IEEE Spectrum, 32-38 (1990).
5. T.Suzuki, “ *Perpendicular magnetic recording-its basics and potential for the future*”, IEEE Trans. on Magnetics, **Mag-20**, 675-680 (1984).
6. D.E Speliotis, “ *Media for high density Magnetic Recording*”, IEEE Trans. on Magnetics, **Mag-20**, 669-674 (1984).
7. S. Iwaski, “ *Perpendicular magnetic recording-evolution and future*”, IEEE Trans. on Magnetics, **Mag-20**, 657-662 (1984).
8. G. Bate, “*Particulate recording materials*”, Proceedings of IEEE, **74** 1513-1524 (1986).
9. B.C Pear, “ Magnetic recording ”, Reinhold Publishing Corporation, p.48 (1967).
10. D.F Eagle and J.C Mallinson, “ *On the coercivity of γ -Fe₂O₃ particles*”, J. Applied Physics, **38**, 995-997(1967).
11. U.Kullman, E.Koster and B. Meyer, “ *Magnetic anisotropy of Ir- doped CrO₂*”, IEEE Trans. on Magnetics, **Mag-20**, 742-744, (1984).
12. S.Umeki, “*A new high coercivity magnetic particle for recording tape*”, IEEE Trans. on Magnetics, **Mag-10**, 655-656 (1974).

13. P.G. Prasad, "*Studies of metal substituted barium ferrites synthesized by a novel auto-ignition method for ultra high density recording applications*", M.Tech. thesis, Indian Institute of Technology, Kanpur, 1998.
14. H. Kojima in, "Ferromagnetic materials- A hand book on the properties of magnetically ordered substances, E.P Wohlfarth (Editor), **3**, North Holland, Amsterdam, 1987, p. 305-391.
15. G. Albanese, "*Recent advances in hexagonal ferrites by the use of nuclear spectroscopic methods*", J. De Physique, **CI-85**, 1977.
16. B.D. Cullity, "Introduction of magnetic material" Addison-Wesley, London (1972), p. 198
17. X.Z. Zhou, A.H. Morrish and Z.W. Li, "*Site preference for Co^{2+} and Ti^{4+} in Co-Ti substituted barium ferrite*", IEEE Trans on Magnetics, **27**, 4654-4656 (1991).
18. T.C Arouldsussen, "*Thin film recording media*", Proc. of IEEE , **74**, 1526-1539 (1986).
19. W.A. Kaczmark and B.W. Ninham, "*Magnetic properties of barium ferrite powders prepared by surfactant assist ball milling*", IEEE Trans. on Magnetics, **30**, 717-719 (1994).
20. J.P.Chen, C.M.Sorensen, K.J.Kalbunde, G.C.Hadjipanayis, E.Devlin and A.Kostikas, "*Size-dependent magnetic properties of MnFe_2O_4 fine particles synthesized by coprecipitation*" **54**, Physical Review B, 9288-9296 (1996).
21. I.J. McColm and N.J. Clark, "Foaming, shaping and working of high performance ceramics", Blackie Glasgow, 1988, p-1.
22. P.Gornert, E.Sinn, W.Schuppel, H. Pfeiffer, M. Rosler, Th. Schubert M. Jurisch and R. Sellger "*Structural and magnetic properties of $\text{Ba}_{12-2x}\text{Co}_x\text{Ti}_x\text{O}_{19}$ powder prepared by glass crystallization method*", IEEE Trans. on Magnetics, **26**, 12-14 (1990).

23. G. Turrilli, F. Licci, S.Rinaldi and A. Deriu, "*Mn²⁺, Ti⁴⁺ substituted barium ferrite*" J. Magnetism and Magnetic Materials, **59** (1986) Amsterdam, 127-131.
24. O.Kubo, T.Ido, H.Yokoyama, and Y.Koike, "*Particle size effect on a magnetic properties of BaFe_{12-2x}Ti_xCo_xO₁₉*" J.Appl.Physics **57**, 4280-4282 (1985).
25. P. Sujatha Devi and H.S. Maiti, "*A novel autoignition combustion process for the synthesis of Bi-Pb-Sr-Ca-Cu-O superconductors with T_c(0) of 125K*", J.Solid State Chemistry, **109**, 35-42 (1994).
26. JCPDS- *diffraction data*. **39**-1433, 1996.
27. JCPDS- *diffraction data*. **44**-1485, 1996.
27. D.G Agresti ,T.D. Shelfer,Y.K Hong and Y.J Paig "*A Mossbauer study of CoMo- substituted barium ferrite*", IEEE Trans. on Magnetism ,**25** 4069-4071 (1989).
28. M.V. Rane, D. Bahadur, S.D Kulkarni and S.K. Date, "*Magnetic properties of NiZr substituted barium ferrite*" J.Magnetism and Magnetic Material, **195**, 1999, L256-L260.
30. D.K Rai, "*Preparation and Characterization of cobalt and cobalt-titanium substituted barium ferrites for magnetic recording*", M.Tech. thesis, Indian Institute of Technology, Kanpur, 1999.
31. G. Turrilli, F. Licci, A. Paoluzi and T. Besagni, "*NiTi substituted hexaferrites for Magnetic Recording*", IEEE Trans. on Magnetism, **24** 2146-2149 (1988).